21

Interaction of Light with Botanical Specimens

Ping-Chin Cheng

INTRODUCTION

In recent years, plant biotechnology has become an important sector, with the agricultural and pharmaceutical industries promoting research activities in plant sciences. This has placed increased demands on sophisticated optical microscopy to assist plant research. While most of the discussion of confocal and multiphoton fluorescence microscopy concentrates on the imaging of animal tissues and cells, very little attention has been paid to the imaging of botanical specimens. As a result, plant researchers frequently have to rely on the imaging technology developed primarily from animal work. While there is nothing wrong with using suitable technology developed for other systems, in this case allowance must be made for the optical characteristics of botanical specimens. Unlike animal cells, plant cells are designed to interact with light, either to harvest energy or to protect sensitive organelles. As a result, plant cells are generally more optically active and heterogeneous and contain significantly more absorbing, scattering, and fluorescent structures. In addition, many botanical specimens exhibit birefringence and are also capable of generating strong second and third harmonic signals.

The specimen is an integral part of any microscope system and its optical characteristics directly affect the performance of the microscope. To image botanical specimens effectively, one must first understand their optical properties. Plant tissues are generally bulkier than their animal counterparts and their cells are usually larger. As most plant cells contain a significant number of fluorescent molecules tightly coupled to the photosynthetic system, they interact with the illumination very differently from animal cells.

Optical microscopy is likely to cause significant disturbances to the physiology of plant cells. For example, the autofluorescence intensity and spectra varies with the duration and intensity of the illumination (Cheng *et al*., 2000a; 2001). This chapter discusses the various optical and fluorescence properties that affect the optical microscopy of plant specimens. A number of plant tissues, both photosynthetic and non-photosynthetic, will be used to illustrate the imaging characteristics of botanical specimens, including their ability to produce useful and informative contrast using second and third harmonic generation signals (SHG and THG). In addition, the methods suitable for imaging various plant organs and tissues are discussed.

LIGHT ATTENUATION IN PLANT TISSUE

The **transmission** of light incident on plant tissue is mainly determined by the amount of absorption and scattering in the specimen. Because it is technically difficult to separate these two factors, we will refer to their joint effects as attenuation. In this article, we estimate attenuation using a detector equal to the size of a parallel illumination beam and placed behind a specimen with a detecting solid angle no larger than 5°. The measured transmission intensity (I_{tran}) is approximated as

$$I_{tran} = I_0 - I_{abs} - I_s$$

where I_0 is the incident intensity, I_{abs} is the intensity lost due to absorption, and I_s is the decrease of transmitted intensity due to light scattering out of the beam.

Linear Absorption

As water is the most abundant material in living systems, light absorption of water determines the usable spectral range of optical microscopy of living material. Figure 21.1 shows the absorption spectrum of water from 200 to 1400 nm. Note that water is transparent at the shorter wavelengths, with two minor absorption peaks at approximately 1000 and 1200 nm, but becomes opaque at wavelengths longer than 1300 nm. Besides water, botanical tissue consists of organic molecules similar to those found in animal tissue, plus cellulose, chlorophylls, anthocyanins, flavonols, lignin, sporopollenin, polyesters (cuticle), starch, inorganic deposits, and other light absorbing pigments. The pigments can play havoc with labeling studies while cellulose structures scatter and refract the light. Fortunately, the latter problem is really a cloud with a "silver lining" because such structures are also very efficient at producing SHG and THG signals.

Figure 21.1 shows the attenuation spectra of plant tissue (rice leaf, *Oryza sativa*) and animal tissue (chicken dermis). Compared to animal tissue, plant tissue, particularly photosynthetic tissue, has significantly higher absorbance in the visible spectrum but similar attenuation in the near infrared (NIR) range. It is evident that the most transparent region of both animal and plant tissue is around 1300 nm. Figure 21.2 shows the attenuation spectra of a number of other plant tissues including maize leaf (green), etiolated maize leaf (yellow), carrot (orange), and rose petal (red).

Ping-Chin Cheng • State University of New York, Buffalo, New York 14260 and Department of Biological Sciences, National University of Singapore, Singapore

 Handbook of Biological Confocal Microscopy, Third Edition, edited by James B. Pawley, Springer Science+Business Media, LLC, New York, 2006.

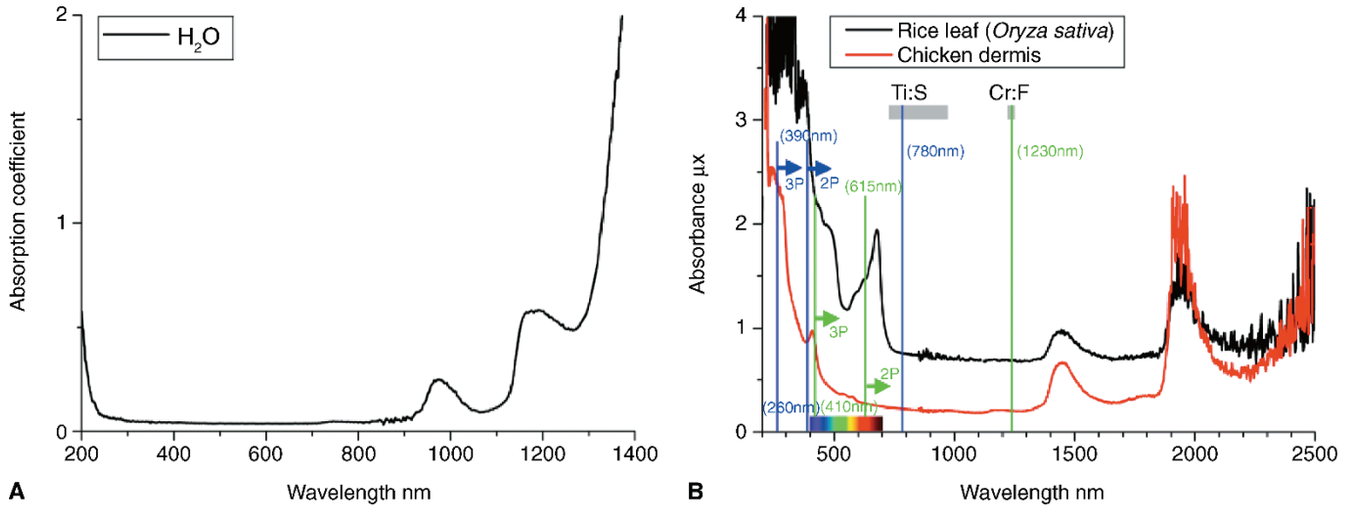

FIGURE 21.1. Absorption spectrum of water (A) and attenuation spectra of living rice leaf (*Oryza sativa* L.) and chicken dermis (B). The low absorption ($\mu < 0.5$) window of water between 200 to 1300 nm determines the useful range of optical microscopy for living biological specimens. Water becomes opaque for wavelengths longer than 1300 nm. Note that, while the photosynthetic pigments in plant tissue produce additional absorption peaks in the blue and red region not found in animal tissue, both types of specimen show little attenuation in the NIR. The blue and green lines show the typical operating wavelengths of Ti:sapphire and Cr:forsterite lasers, respectively. The *colored arrows* indicate the upper limit of two- and three-photon excitation. The gray bars indicate the tuning range of the respective lasers.

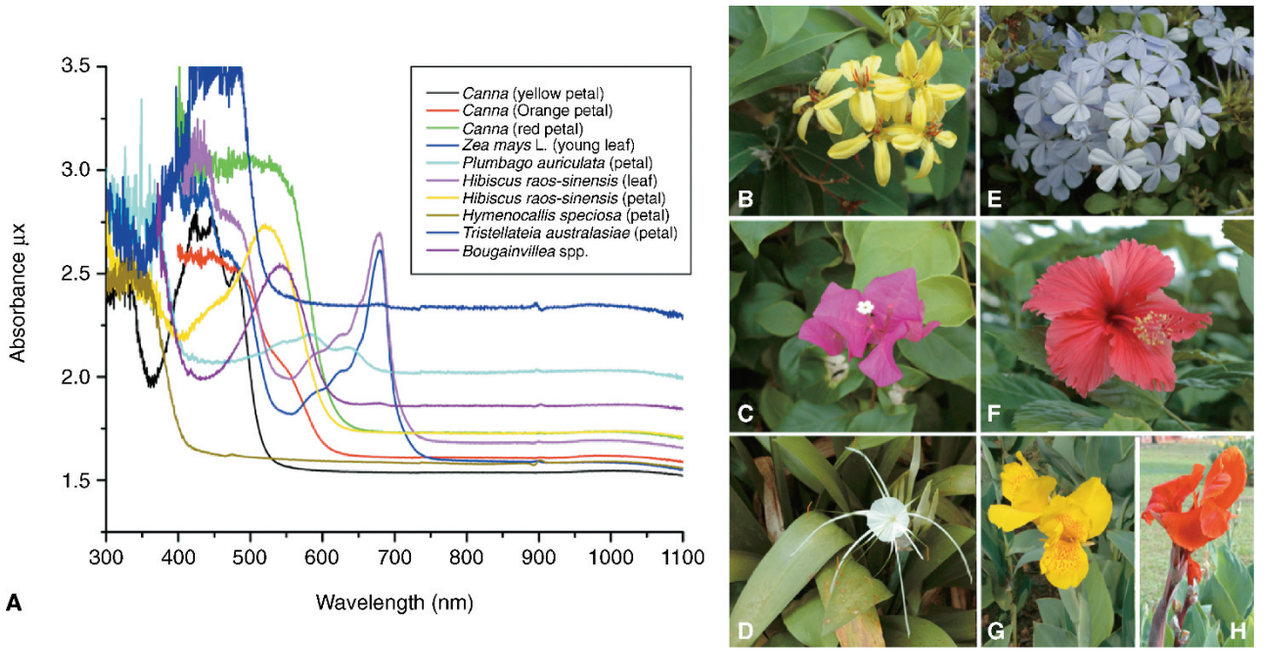

FIGURE 21.2. Attenuation spectra of various plant petals and leaves.

Using *Arabidopsis thaliana* leaf as an example, Figure 21.3(A) is an attenuation spectrum showing a general increase in optical density towards the shorter wavelengths. Two prominent absorption peaks are contributed by leaf pigmentation, mainly the chlorophylls. The attenuation spectrum of an acetone-extracted, pigment-free leaf shows the removal of both peaks and lower overall attenuation [Fig. 21.3(B)]. Figure 21.3(C) shows the attenuation of protoplasts in culture medium (ca. 2×10^4 cells/mL). Because the light-scattering cell wall is now absent, the attenuation at 400 nm is very similar to that at 1000 nm. However, in the more fibrous *Marsilea quadrifolia* leaf, where scattering is significant, removal of the pigments does little to lower the light attenuation (Fig. 21.4). It is worth noting that, over the spectral range of 520 to 850 nm, the light attenuation is very similar in the leaves of both species. These spectra show that using NIR (700–900 nm) illumination for multi-photon microscopy offers only a limited penetration advantage over the shorter wavelength light used in single-photon excitation. Although a significant increase in penetration depth can be gained by using wavelengths in the 1200 nm range (Fricker *et al.*, 1992; White *et al.*, 1996; Lin *et al.*, 2000c, 2001; Chu *et al.*, 2003a), resolution will be lower because of the longer wavelength and because most objectives are corrected only for visible light. On the other hand, if the refractive index (RI) of a sample does not match that of the medium in which it is immersed, the use of a longer wavelength often reduces the aberrations caused by this mismatch (because all RIs drop with wavelength and the differences between the RIs of the different components become smaller), and this factor compensates somewhat for the loss of resolution.

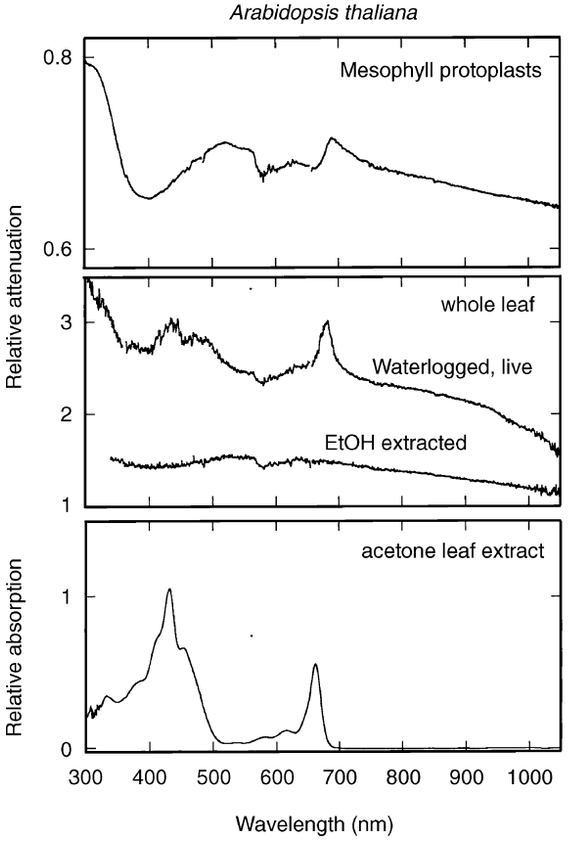

FIGURE 21.3. Attenuation spectra of (A) *Arabidopsis thaliana* protoplast, (B) water-logged whole leaf and EtOH-extracted leaf, and (C) acetone-extracted leaf.

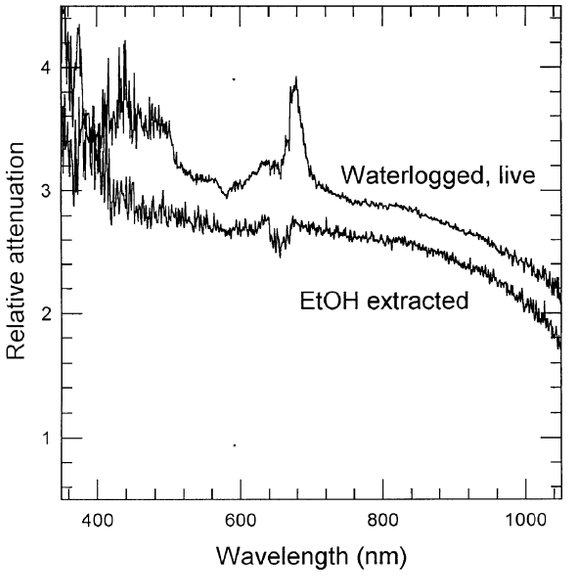

FIGURE 21.4. Attenuation spectra of a living leaf of *Marsilea quadrifolia* and after ethyl alcohol extraction.

In addition to the 700 to 1300 nm region, green plant tissue shows a secondary low attenuation window around 550 nm. Selecting a flurophore with an emission peak within this region improves the detectable fluorescence signal as long as there is no overlapping autofluorescence. In addition, the 550 nm region is suitable for backscattered light (BSL) imaging within the visible spectrum. Fluorochromes with their fluorescence emission longer than 650 nm, such as Alexa Fluor 680, Alexa Fluor 750, Cy5.5, and Cy7 (Molecular Probes Inc.), can be very useful for botanical specimens. In this spectral region, the absorption of plant material is low, relatively little autofluorescence is produced, and the signal is still suitable for high quantum efficiency (QE), Si-based photodetectors.

Nonlinear Absorption

In nonlinear optics, the nonlinear optical response can be described by the power series

$$\begin{aligned}\tilde{P}(t) &= \varepsilon_0\chi^{(1)}\tilde{E}(t) + \varepsilon_0\chi^{(2)}\tilde{E}(t)^2 + \varepsilon_0\chi^{(3)}\tilde{E}(t)^3 + \ldots \\ &\equiv \tilde{P}^{(1)}(t) + \tilde{P}^{(2)}(t) + \tilde{P}^{(3)}(t) + \ldots\end{aligned}$$

where $\chi^{(2)}$ is the the second-order nonlinear susceptibility and $\chi^{(3)}$ is the third-order nonlinear susceptibility.

Although the nonlinear optical response of man-made materials has been extensively studied, the nonlinear absorption properties of plant specimens are poorly understood. Figure 21.5 shows a transmission versus incident intensity curve of a flurophore (APSS; Cheng *et al.*, 1998) at 780 nm. Although the absorption increases as the incident power increases, one should note that a specimen showing little absorbance in the NIR may exhibit significant nonlinear (two-photon) absorption at high peak illumination intensity, and significant energy can thus be absorbed by the specimen. This is the case for the chloroplast. Even though the APSS fluorophore shows low absorbance in the NIR region, significant two-photon absorption is evident. The shaded bar in Figure

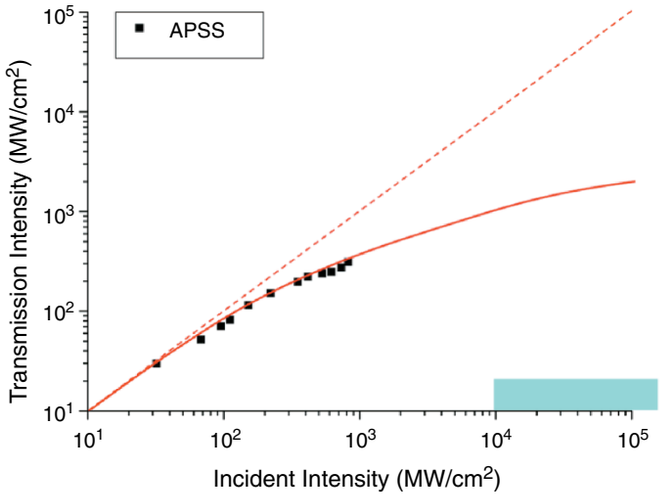

FIGURE 21.5. Nonlinear absorption of APSS fluorophore solution. The *light blue bar* represents the range of power densities used in a typical multi-photon fluorescence microscopy setup, In general, higher power density occurs when a high-NA objective is used because the focal spot is smaller.

21.5 represents the power density used in a typical multi-photon fluorescence microscope. Under high power density IR illumination, significant cellular damage can result (Konig *et al.*, 1995, 1996a,b, 1997; Oehring *et al.*, 2000; Chapter 38, *this volume*; and see paragraph below on light–specimen interactions).

Scattering

Both Rayleigh and Mie scattering occur in botanical specimens. Rayleigh scattering is produced by small particles (less than a tenth of the wavelength) and is more effective at shorter wavelengths; the intensity of the Rayleigh-scattered light I is

$$I = I_0 \frac{8\pi^4 N\alpha^2}{\lambda^4 R^2}(1+\cos^2\theta)$$

where N is the number of scatters, α is the polarizability, and R is the distance from the scatterer.

Clearly, Rayleigh scattering is highly wavelength dependent:

$$I \propto \frac{1}{\lambda^4}$$

Therefore, the wavelength-dependent attenuation observed in the spectrum (Fig. 21.6) is mainly due to Rayleigh scattering.

In contrast, Mie scattering predominates for particles that are larger than a wavelength. This scattering produces a pattern similar to an antenna lobe, with a sharper and more intense forward lobe for larger particles. Mie scattering is generated mainly by the organelles in the cell and, while not strongly wavelength dependent, the scattering intensity is proportional to the square of the ratio of the RI of the feature to the RI of the media (see Fig. 8.2, *this volume*). Figure 21.6 shows the contribution of scattering to the light attenuation in hydrated and methyl salicylate–cleared parenchyma cells in a maize stem (Cheng *et al.*, 2001a). By index-matching many of these small particles, the clearing process greatly reduces scattering within a specimen. This allows one to image significantly deeper into the tissue.

In a simulation of biological specimens, Gu and colleagues (2000) have demonstrated that Mie scattering is the dominant scattering event in milk and that, as long as spherical aberration is not a problem, scattering is the determining factor for the depth limit in multi-photon microscopy. Figure 21.7 shows a high-intensity NIR beam incident on a 1 mm cuvet containing diluted (20% dilution) 2% homogenized milk; note the two-photon excited fluorescence in the second cuvet and the scattered NIR in the milk-containing cuvet.

Between the outer layers of epidermal cells, leaves consist mainly of mesophyll tissue, each cell being rich in photosynthetic pigments confined within light-scattering cell walls. The outer surface of epidermal cells is generally covered with a layer of cuticle that has a refractive index significantly different from that of water. As a result, the cuticle surface reflects incident light particularly that impinging at low angles, preventing some of it from entering the leaf and effectively reducing the NA of the objective. The cuticle surface may be covered with a complex surface pattern (Cheng *et al.*, 1979a, 1981, 1986; Cutler *et al.*, 1982), which further increases scattering and lowers the intensity of the illumination penetrating the tissue.

Specialized cells on the leaf surface, such as heavily walled guard cells and silica cells (frequently found in grasses; Jones and Handreck, 1967), provide additional scattering centers that can also significantly attenuate the illumination. Finally, a significant volume of the leaf is occupied by an air space that becomes the major reflection and scattering center within the tissue.

One method commonly used to combat these problems in freshly excised tissue is to soak the leaf in air-deficient culture medium/water (Cheng *et al.*, 2001a) or to place the leaf in water but under a partial vacuum to remove the air trapped in the mesophyll. Air-deficient water is prepared by filling a bottle with boiling water, recapping the bottle when the water is hot and without any trapped air bubbles, and then letting the water cool down. The bubbling and high temperature removes dissolved air. Soaking leaves in this air-deficient water can quickly and efficiently dissolve away air bubbles trapped in tissue without the damage caused when the air trapped in the leaf expands under vacuum. Figure 21.8 shows

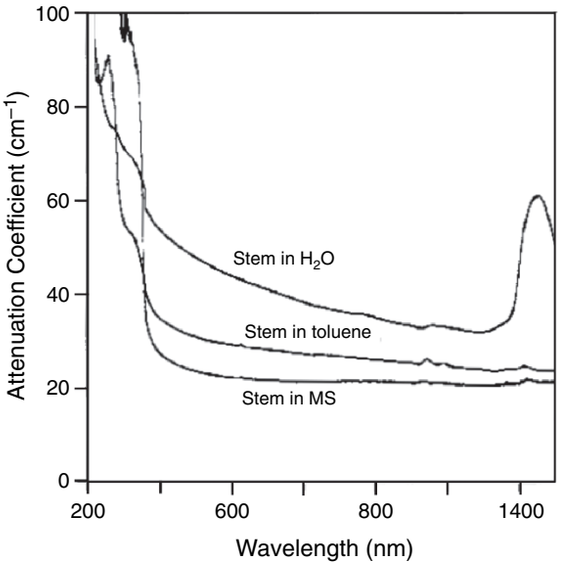

FIGURE 21.6. Attenuation spectra of maize stem (pith) in water, xylene, and methyl salicylate (after dehydration with EtOH). All spectra were obtained from the same spot on the sample.

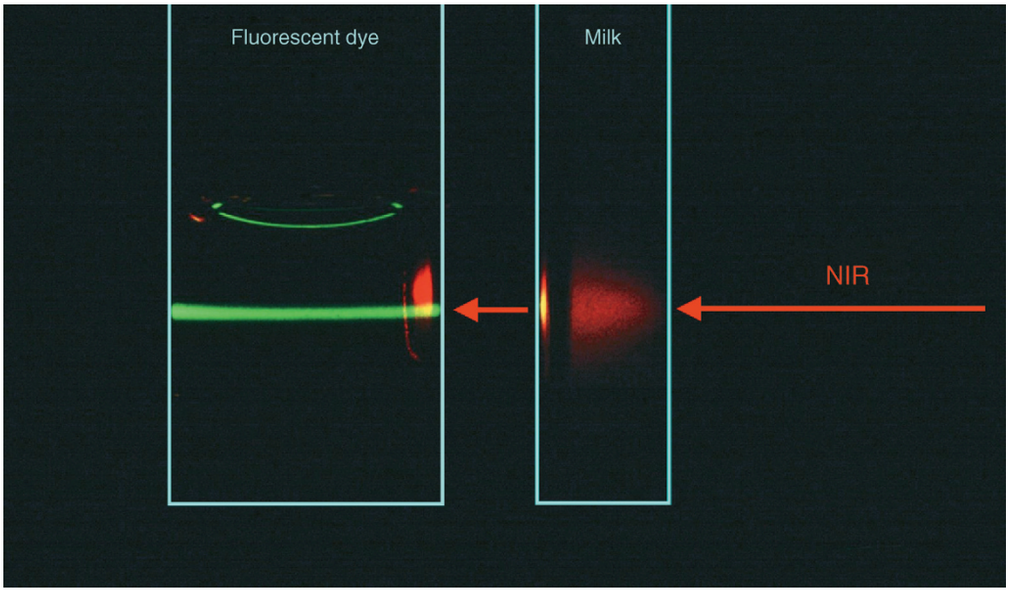

FIGURE 21.7. Demonstration of high penetration of NIR beam in turbid medium. High intensity IR beam incident on a cuvet filled with diluted milk. The ballistic photons leaving the milk are intense enough to excite 2P fluorescence in the dye solution in the second cuvet.

significantly less scattering from waterlogged leaves and this allows an increase in imaging depth.

If living tissue observation is not required, the high scattering of botanical specimens can be minimized by fixation, dehydration, and clearing procedures commonly used in traditional microtechniques. Figure 21.6 demonstrates the effect of such a clearing procedure on the scattering properties of the parenchyma cells of maize stem (pith). Untreated, these cells have no pigmentation and appear white to the naked eye (mainly due to Mie scattering). However, after clearing, the tissue becomes nearly transparent. The absence of the absorption peak at 1450 nm is due to the absence of water.

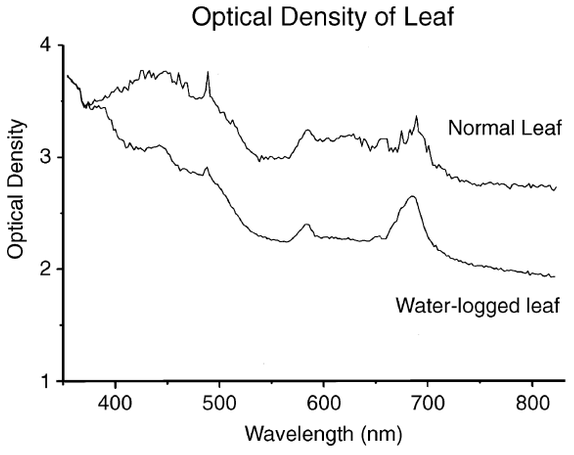

FIGURE 21.8. Attenuation spectra of a live maize leaf before and after being waterlogged. Note the significant decrease in attenuation [nearly 1 optical density (OD) unit in the red] due to the elimination of the air spaces in mesophyll tissue. This significantly improves the penetration of the excitation light in single-photon excitation and also greatly increases the returning fluorescence signal.

REFRACTIVE INDEX HETEROGENEITY

Any optical heterogeneity within the specimen or deviation in the refractive index from the design specification of the objective can produce spherical aberration (Chapter 20, *this volume*). Structures having different refractive indexes can also affect the flatness of an optical section. Recently, spherical aberration introduced by a living specimen has focused attention on the need to process specimens properly to minimize refractive index mismatches within them (Cheng and Cheng, 2001; Cheng *et al*., 2002; Pawley, 2002).

Examples of optical heterogeneity in plant specimens can be demonstrated by laying maize tissue sections on the surface of a slide made of fluorescent plastic (Cheng *et al.*, 2002). Figure 21.9 shows an *xz* image of such a specimen. Refractive index heterogeneity within the tissue slice causes the image of the surface of the fluorescent slide not to be flat as it should be (marked by horizontal line). Figure 21.10 shows *xy*, *xz*, and *yz* views of a submerged leaf of *Marsilea quadrifolia* using two-photon fluorescence microscopy. Note the smearing of the image in the deeper part of the tissue (*xz* and *yz*) as the result of specimen-introduced spherical aberration. Apparently, the depth limit is around 50 to 60 µm in this case. Inspection of the *xz* and *yz* sections reveals that the lower left portions of the *xy* image were obtained near the surface of the specimen while the upper right portion of the image was obtained through 30 µm of tissue. Significant differences in image resolution and signal level are evident.

Historically, this heterogeneity is overcome by dehydration and by clearing and mounting the tissue sections between a slide and coverslip in proper mounting medium. This procedure matches the optical properties of the specimen to the design conditions of the objective lens, and should not be overlooked in modern wide-field, confocal, and multi-photon microscopy. When imaging fixed tissues and cells, always use a clearing agent to reduce scattering and aberrations.

A number of clearing methods are used in optical microscopy, most of them involving the use of organic solvents such as methyl

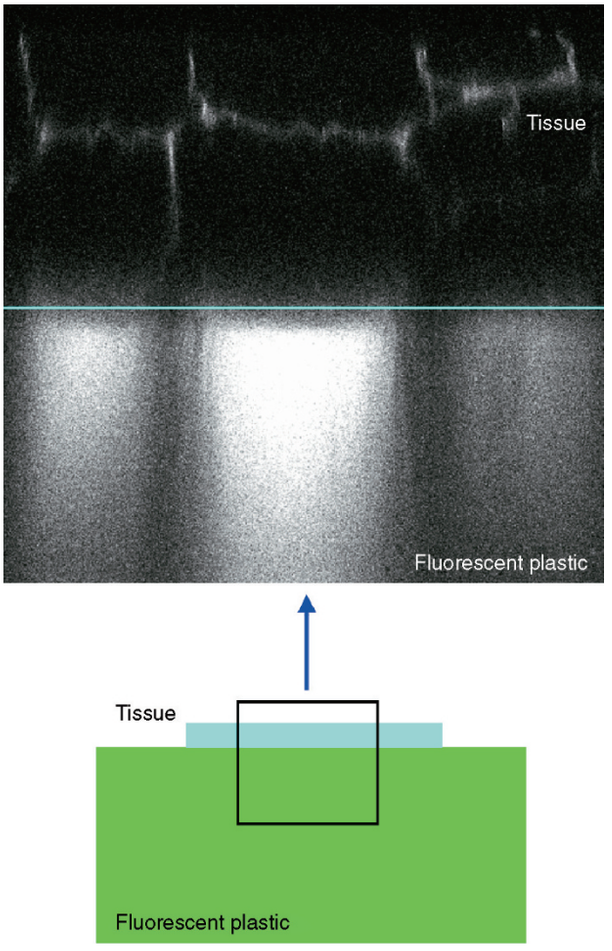

FIGURE 21.9. Optical *xz* section of a piece of maize stem (pith) mounted on a fluorescent plastic slide (Chroma Technology, Inc., and AMIL Technology) showing how the optical heterogeneity of the tissue section dramatically affects the image of the homogeneous fluorescent plastic slide. The horizontal line demarcates the slide surface. Note that the image of the surface of the plastic slide is not flat because RI variations in the overlying section cause the focal length of the relatively low-NA objective to vary.

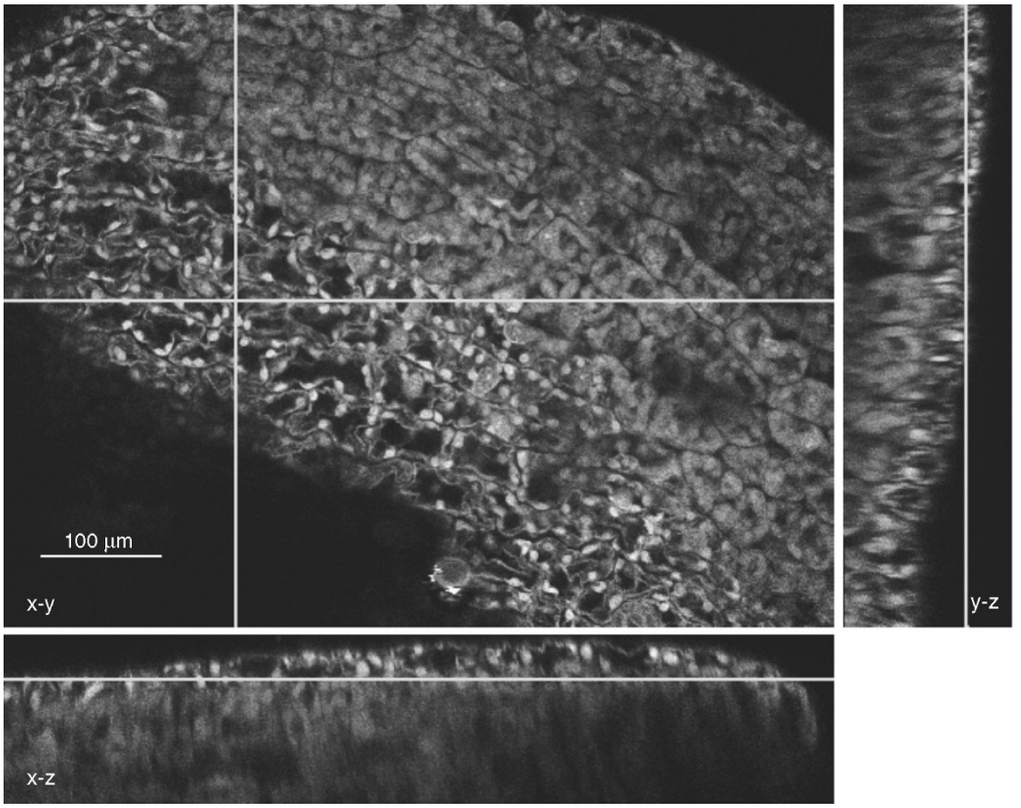

FIGURE 21.10. Two-photon *xy*, *xz*, and *yz* sections of young leaf (the submerged form) of *M. quadrifolia*. The reduction of signal strength and image quality as a function of depth is evident. The *white lines* on the *xy* section indicate the positions where the *xz* and *yz* sections were obtained; similarly, the white lines on the *xz* and *yz* images indicate the corresponding position of the *xy* image. The image was obtained by two-photon fluorescence microscopy of a water-mounted spe-cimen using 800 nm excitation with a water-immersion objective on Olympus Fluroview FV300 confocal microscope.

salicylate ($\eta = 1.52$), xylene ($\eta = 1.5055$), or toludine ($\eta = 1.4961$) (Stelly *et al.*, 1984; Cheng *et al.*, 1993). Examples using methyl salicylate include the study of ovules of *Zephyranthaceae* (Crane and Carman, 1987), grass ovules (Young *et al.,* 1979), and maize apical meristem (Bommineni *et al.*, 1990, 1993, 1995). For hydrated tissue, aqueous based glycerol–Ppda, glycerol ($\eta = 1.4746$) and recently FocusClear ($\eta = 1.43$) and MountClear ($\eta = 1.43$; Pacgen, BC, Canada) can be used in conjunction with Immersion Solution-M ($\eta = 1.43$). All these methods work well with botanical specimens.

In addition to the agents mentioned above, several clearing techniques have been developed for the study of whole-mount plant tissue in the past three decades. These include the BB-4 1/2 clearing fluid (Herr, 1971), the improved BB-4 1/2 (Herr, 1974), and the mixture of benzyl benzoate and dibutyl phthalate (2 : 1, v/v, Crane and Carman, 1987). Examples of the applications of these clearing agents have appeared in many botanical publications, such as the use of Herr's BB-4 1/2 for the study of ovules, pollen, and pollen tubes (Fredrikson, 1992), and the use of benzyl benzoate and dibutyl phthalate mixture in the study of apomixis in *Elymus* (Crane and Carman, 1987). Both Herr's BB-4 1/2 and BB-4 1/2 fluids turn dark brown after 2 to 4 weeks in the light at room temperature because the clove oil photo-oxidizes (Herr, 1992). Because the browning results in a significant increase in light absorbance, it is important to keep the clearing agents in dark bottles and in the refrigerator. Substituting the clove oil with dibutyl phthalate produces a superb photostable clearing agent (Herr's BB-DP-4 1/2; Herr, 1992).

BIREFRINGENT STRUCTURES IN PLANT CELLS

In crystalline materials, it is well known that different refraction indices may be associated with different crystallographic orientations. Mineral crystals frequently show two distinct indices of refraction, and are referred to as birefringent materials. If the *y*- and *z*-directions are equivalent in terms of the crystalline forces, then the *x*-axis is unique and is called the optic axis of the material. The propagation of light along the optic axis is independent of its polarization: its electric field is everywhere perpendicular to the optic axis and is called the ordinary- or o-wave. The light wave with its E-field parallel to the optic axis is called the extraordinary- or e-wave.

Birefringence has to do with anisotropy in the binding forces between the atoms forming the crystal. It can be visualized as the atoms having stronger "springs" holding them together in some crystalline directions than in others. A number of structures in plant tissue exhibit birefringence. These include microtubules, spindles, secondary cell wall, cuticle, surface wax, starch granules, and SiO_2 deposits (bio-opals). For example, paracrystalline cellulose in the cell walls of trichomes of *Arabidopis thaliana* shows birefringence (Brininstool, 2003). Figure 21.11 shows the birefringent properties of maize starch granules as observed under a conventional polarization microscope.

Placing a birefringent material between a pair of crossed polarizers gives rise to interference colors. When light passes through a polarizer to produce linearly polarized light and that light then passes through a piece of birefringent material, the light is broken up into two components. Because the index of refraction for one of them is larger than for the other, that component will lag in phase (retardance) and these components will emerge from the specimen out of phase with each other. Then if the light is passed through a crossed polarizer (the analyzer), only the part of each component that is in the transmission plane of the analyzer will emerge. This emerging ray consists of two co-planar components that differ in phase. If the refraction indices of the material also change with wavelength, then for a given thickness of birefringent material, some wavelengths will undergo destructive interference and some constructive, giving an interference pattern of changing colors similar in appearance to the interference colors of a thin film of oil floating on water. If monochromatic light is used, interfer-

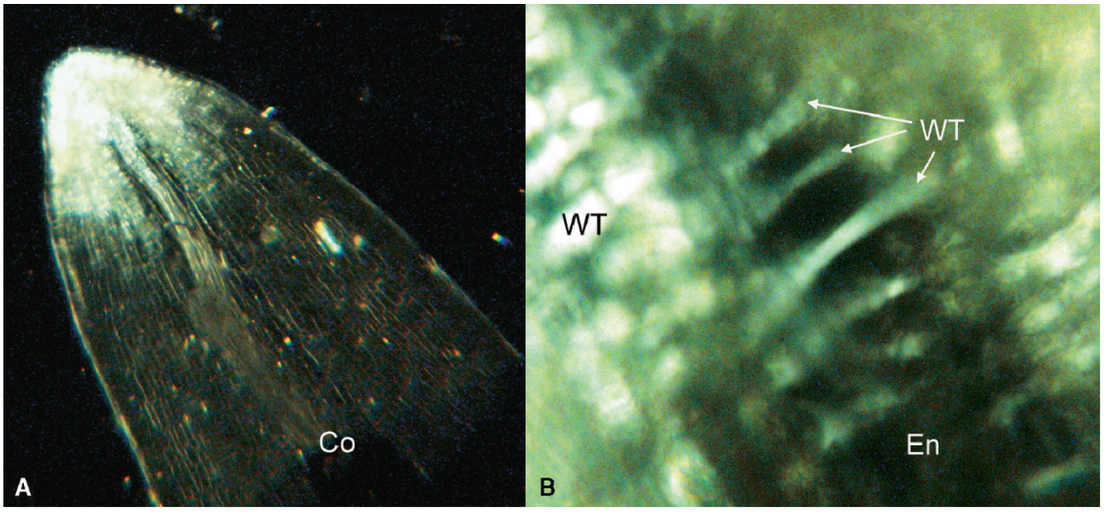

FIGURE 21.11. Birefringent properties in the secondary wall thickenings in the endothelium cells of maize anther.

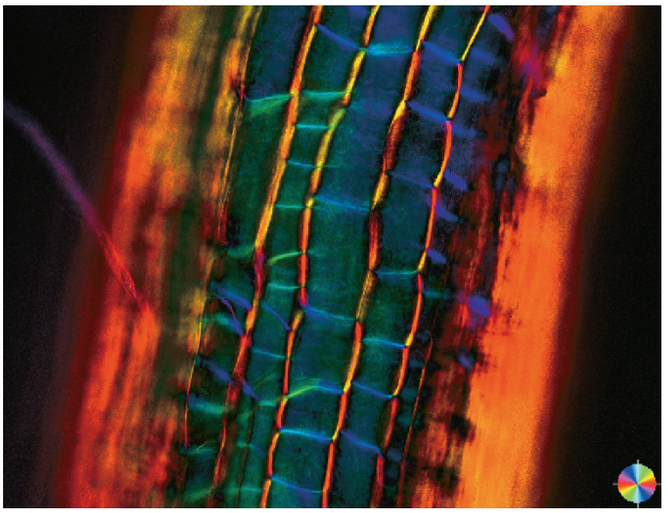

FIGURE 21.12. Dynamic polarization microscopy showing the cell wall orientation (color-coded wheel shows *s*-axis) in the root of *A. thaliana*. The images were obtained by using Polscope. (Images courtesy of Cambridge Research Instruments, Woburn, MA.)

ence fringes are produced. These interference color/fringes can be used to study the thickness and internal stress of plant cuticles (i.e., photoelasticity).

The use of either a conventional or a dynamic, tunable polarization microscope (Polscope, Cambridge Instrument Inc.) can provide image contrast specific to birefringent structures such as the microtubules in the mitotic spindle during cell division. Because of the nature of transmission polarization microscopy, only low intensity light is required, which minimizes phototoxicity. However, as the retardance of many botanical structures, such as cell walls and starch granules, are relatively large, contrast produced by low retardance structures such as microtubules (MT) (typical retardance for a single MT is 0.07 nm) often becomes lost in the high background retardance contributed from the cell wall. Figure 21.12 shows the orientation of cellulose microfibrils in the root cell wall of *A. thaliana*. The cellulose microfibril shows excellent birefringence contrast. The color indicates the orientation of the microfibril molecules.

FLUORESCENCE PROPERTIES OF PLANTS

Plant tissue generally contains a large number of light-absorbing pigments, including those responsible for photosynthesis. Many of these pigments produce autofluorescence (Figs. 21.13, 21.14, and 21.15). Figure 21.13 shows a collection of fluorescence spectra excited at different wavelengths from various plant specimens. Note the spectral variation as the excitation wavelength changes. Figure 21.14 shows the fluorescence spectrum of maize leaf grown in either normal lighting or dark (etiolated) conditions, while Figure 21.15 demonstrates the fluorescence spectra of a methanol extract of etiolated maize leaf at various excitation wavelengths. Because plant tissue consists of a mixture of many fluorescent compounds, each with different absorption spectrum and quantum yield (QY), the resulting fluorescence spectra can vary greatly when subject to different excitation wavelengths. As these endogenous fluorophores produce high intensity background autofluorescence throughout the entire visible spectrum, it is very difficult to separate their output from that emitted by introduced fluorescent probes.

Even worse, the emitted autofluorescence is often so intense that it can, in turn, excite nearby fluorescent tags at a wavelength different from the applied illumination. Therefore, the apparent spectral fingerprint of a fluorescent dye may vary depending on the presence or absence and the location of nearby autofluorescing structures. An example might be the vacuole found in many flower petals. Vacuoles can contain large amounts of anthocyanins and flavonols that produce intense autofluorescence, the emission spectra of which varies according to local pH and ionic conditions. Any fluorescently labeled organelle near the vacuole may be excited by this autofluorescence. Figure 21.16 shows an *xz* section of the petal of tree peony (*Paeonia suffruticosa*), the green channel is the BSL image and the red channel is the autofluorescence image.

Changes in Emission Spectra Depending on One- Versus Two-Photon Excitation

When subjected to excitation illumination at 380 nm, the living, freshly excised leaves of *A. thaliana* emit both strong red fluorescence peaks at 684 nm and 714 nm and blue-green fluorescence in the range of <550 nm [Fig. 21.17(A)]. In contrast, high intensity excitation by 760 nm NIR illumination produces a significantly different upconverting fluorescence spectrum, as shown in Figure 21.17(B). The green and red fluorescence now peaks at 500 nm and 688 nm, respectively. Under 380 nm excitation, the mesophyll protoplasts of *A. thaliana*, exhibit strong red fluorescence, peaking at 680 nm, and very low broadband emission in the 450 to 550 nm range [Fig. 21.17(C)]. The two-photon–excited fluorescence spectrum of these protoplasts is similar to that obtained from the whole leaf but with the 688 nm peak blue-shifted to approximately 660 nm [Fig. 21.17(D)]. It is important to note that the fluorescence emission spectra generated by the excitation with single-photon excitation is not identical to that produced by two-photon excitation at double the wavelength. Kennedy and Lytle (1986) have also reported a difference between the excitation spectra obtained from single-photon and two-photon excitation. Therefore, two-photon images may well be different from those obtained from single-photon excitation with half of the wavelength.

Microspectroscopy

Because of the complexity of plant autofluorescence, it is frequently advisable to obtain fluorescence spectra from the organelles of interest to confirm their fluorescence signature. This can be achieved using either single-photon or two-photon microspectroscopy (Cheng and Cheng, 2000; Kao *et al.*, 2000a,b; Chu *et al.*, 2001). The latter has the advantage of providing excellent three-dimensional spatial resolution of the location from which the fluorescence spectra can be obtained.

This technique can also be used to separate SHG and THG signals from background fluorescence (Sun *et al.*, 2001). Figure 21.18 shows the setup of a home-built microspectroscopy system [Fig. 21.18(A)] and a fluorescence spectrum of a parenchyma cell in maize stem [Fig. 21.18(B)]; the spectrum was obtained by two-photon excitation (λ_{ex} = 800 nm) from the fluorescent spot indicated by the arrow in Figure 21.18(C). The setup consists of a linear charge-coupled device (CCD)-equipped (Roper Scientific) Acton 2300i spectrometer connected to the photo port of an Olympus IX70 inverted microscope via a fiber bundle. A

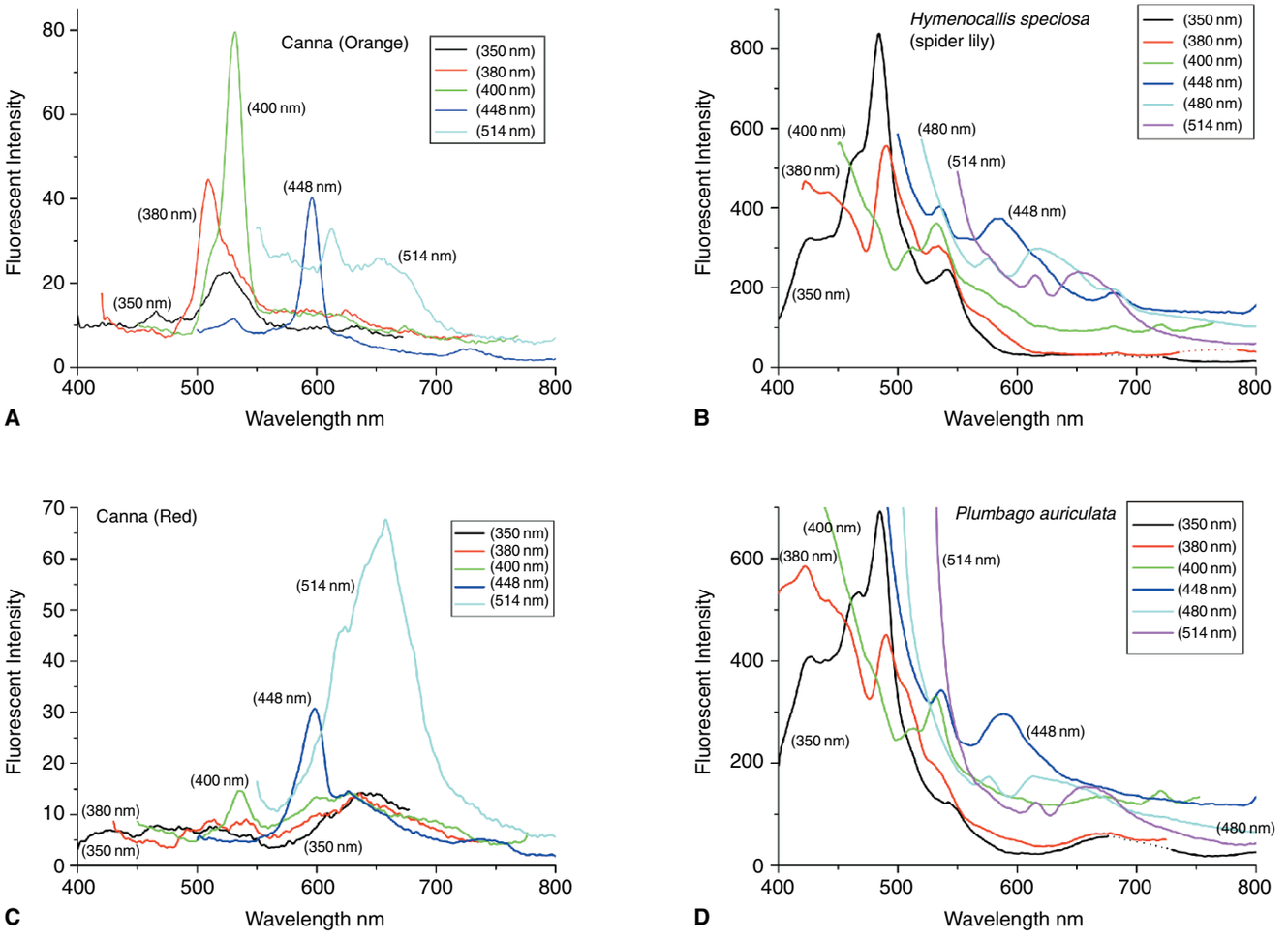

FIGURE 21.13. (A–D) Comparative fluorescence spectra of various plant materials [the petal of yellow, orange, and red varieties of *Canna* L., spider lily (*Hymenocallis speciosa*) and forget-me-not (*Plumbago auriculata*)]. The interruption in the spectra (*dashed line*) is the estimated spectrum as the data were contaminated by scattered excitation illumination leaving the spectrometer grating as a 2nd order diffraction peak.

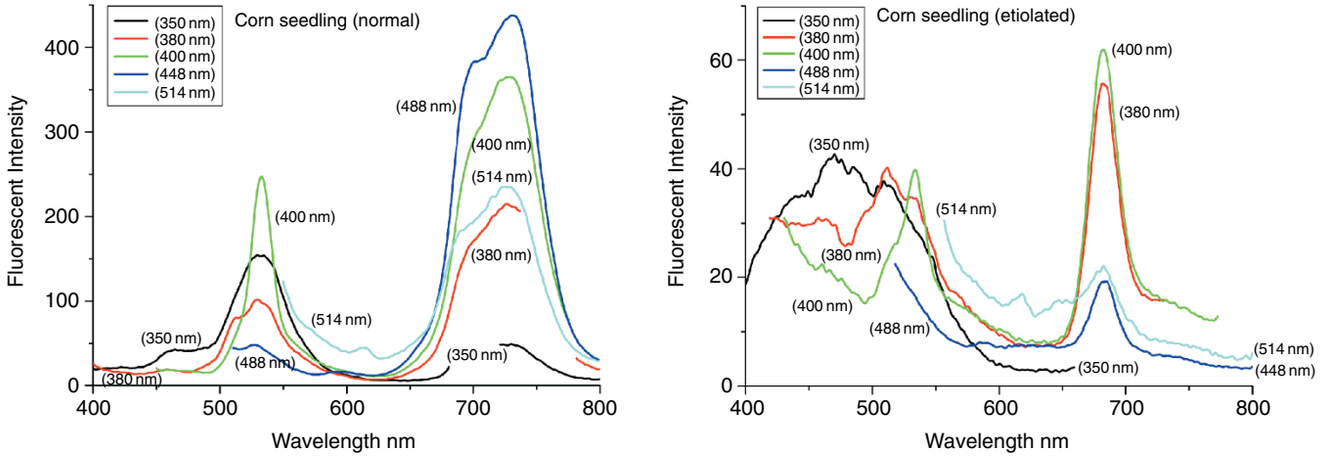

FIGURE 21.14. Autofluorescence spectra of normal and etiolated maize seedling (*Zea mays* L., var. Golden Beauty) excited by light at different wavelengths.

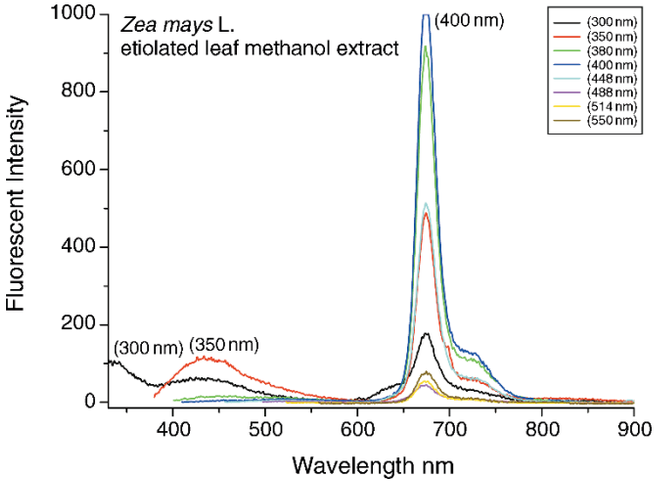

FIGURE 21.15. Fluorescence spectra of the leaf methanol extract obtained from etiolated maize seedlings (*Zea mays* L., var. Golden Beauty) shows significant change in fluorescence spectra when excited by different excitation wavelengths.

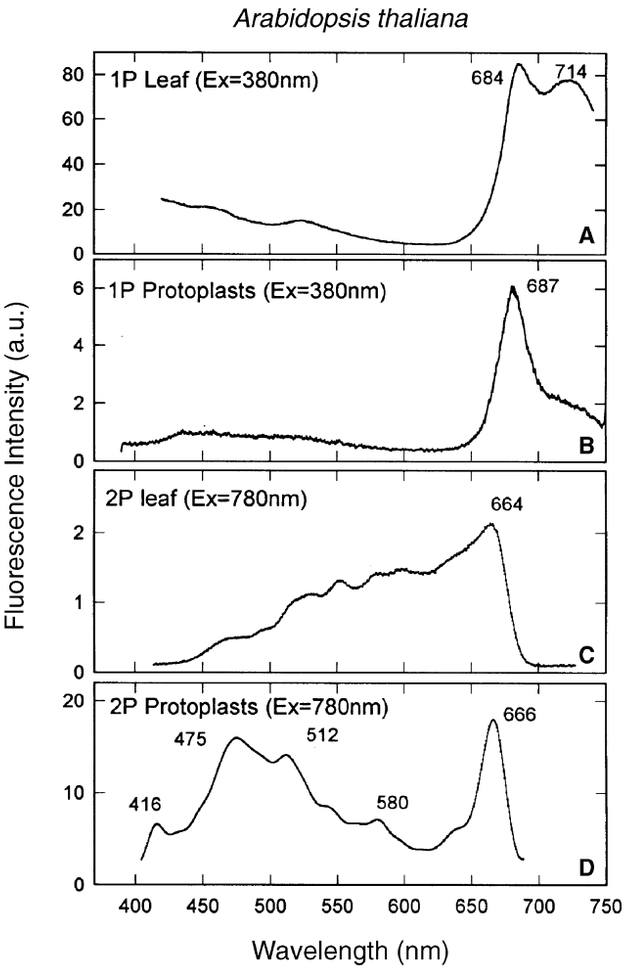

FIGURE 21.17. Comparison of fluorescence spectra obtained with single-photon and two-photon excitation in a leaf preparation of *A. thaliana*. (A) Single-photon excited fluorescence spectrum of fresh, untreated leaf, excited at 380 nm, (B) fluorescence spectrum of mesophyll protoplasts excited with 380 nm, (C) two-photon fluorescence spectrum of leaf excited at 780 nm, (D) two-photon fluorescence spectrum of protoplast excited at 780 nm. (Ti:Sa mode-lock laser operated at 82 MHz, 100 fs pulse at an average power of 600 mW, beam diameter approximately 0.8 mm in diameter.)

mode-lock ultra-fast titanium–sapphire laser was used as the light source for two-photon fluorescence excitation.

A number of modern confocal microscopes are capable of recording fluorescence spectra and these should be used to understand the fluorescence signature and photobleaching dynamics of the specimen under study. Figure 21.19 shows an example of spectra of a living maize chloroplast as a function of light exposure. The three dimensional (3D) spectra (intensity vs. wavelength vs. time) demonstrates the evolution of chloroplast fluorescence when it is subjected to light at high enough intensity to cause significant radiation damage (Konig *et al*., 1995, 1996a, 1997; Cheng *et al*., 2000a, 2001; Kao *et al*., 2000b; Lin *et al*., 2000a,b; Chen *et al*., 2002).

Fluorescence spectra obtained from botanical specimens are generally contributed by the emission of many fluorophores, frequently with overlapping emission peaks. There are a number of methods to separate/minimize the overlapping spectra, such as sequentially exciting the specimen with various excitation wavelengths or using spectral unmixing techniques.

The term *spectral unmixing* refers to a series of computer algorithms that are used to separate a spectral signal recorded from a single pixel or a defined area containing a number of fluorophores into separate intensity signals for each one of them. The algorithms vary depending on the hardware used to initially record the spectral data but all of them have a close similarity to the programs used to deconvolve 3D widefield data or data from energy-dispersive X-ray spectrometers (EDS) in electron microscopy. In spectral unmixing, the spectrum of each individual dye serves as if it were one of a series of "point-spread functions" and it is the function of the unmixing algorithm to make the best fit between the recorded data and a weighted sum of the emission spectra of the dyes (i.e., each one acting like a "PSF" with a shape and a position) thought to be present. This is based on the assumption that the spectra of the individual dyes are not changed by their being combined in the pixel or area of interest (i.e., that micro-environmental differences are either absent or inconsequential). On the other hand, it is common to use signal from a nearby pixel(s) that is felt to be producing only background autofluorescence, as the reference to unmix the pixel of interest and obtain a background-free spectrum. This assumes that the reference background also represents the background present in the measured pixel(s).

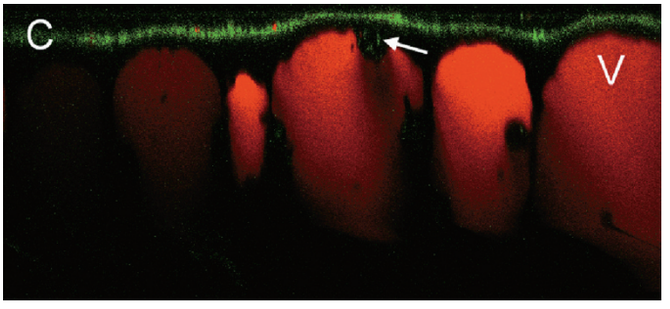

FIGURE 21.16. Two channel (backscattered light and autofluorescence) confocal *xz* section of a tree peony *(Paeonia suffruticosa)* petal.

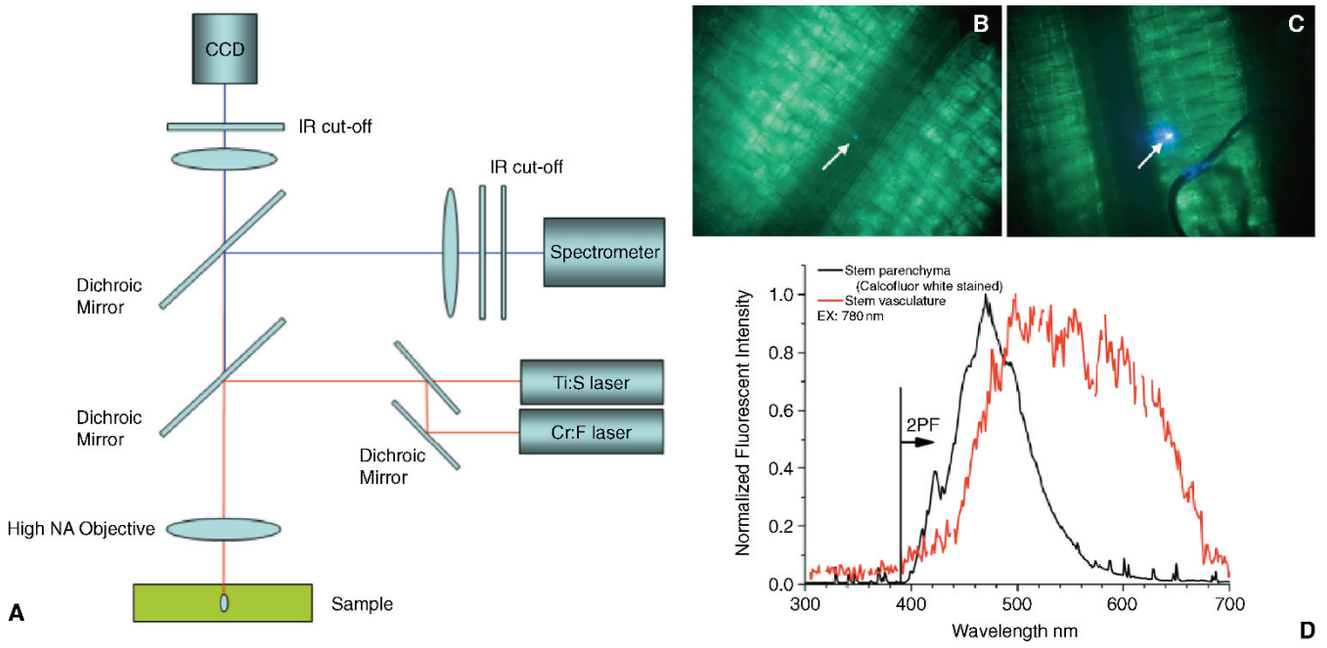

FIGURE 21.18. (A) A multi-photon microspectrometer setup, (B) two-photon excited fluorescent spot (*arrow*) in a maize stem, (C) two-photon excited fluorescent spot (*arrow*) in a maize stem stained with Calcofluor white, and (D) the recorded fluorescence spectra.

For example, it is difficult to detect green fluorescent protein (GFP) expression in chloroplasts because the chloroplast contains not only strongly fluorescing chlorophylls, but also the many highly fluorescent associate pigments of the photosynthetic apparatus, some of which emit in the green region. Exciting each fluorophore sequentially with the appropriate excitation wavelengths may also be helpful in reducing the problem of crosstalk between detection channels. Unfortunately, multi-photon excitation generally causes all fluorophores to fluoresce, creating broadband fluorescence emission for which the only really effective antidote is unmixing (Figs. 21.13 and 21.14).

Figure 21.20 demonstrates the use of spectral unmixing in conventional transmitted and epi-fluorescence microscopy of the rhizome of lily of the valley (*Convalaria majalis*) to separate the

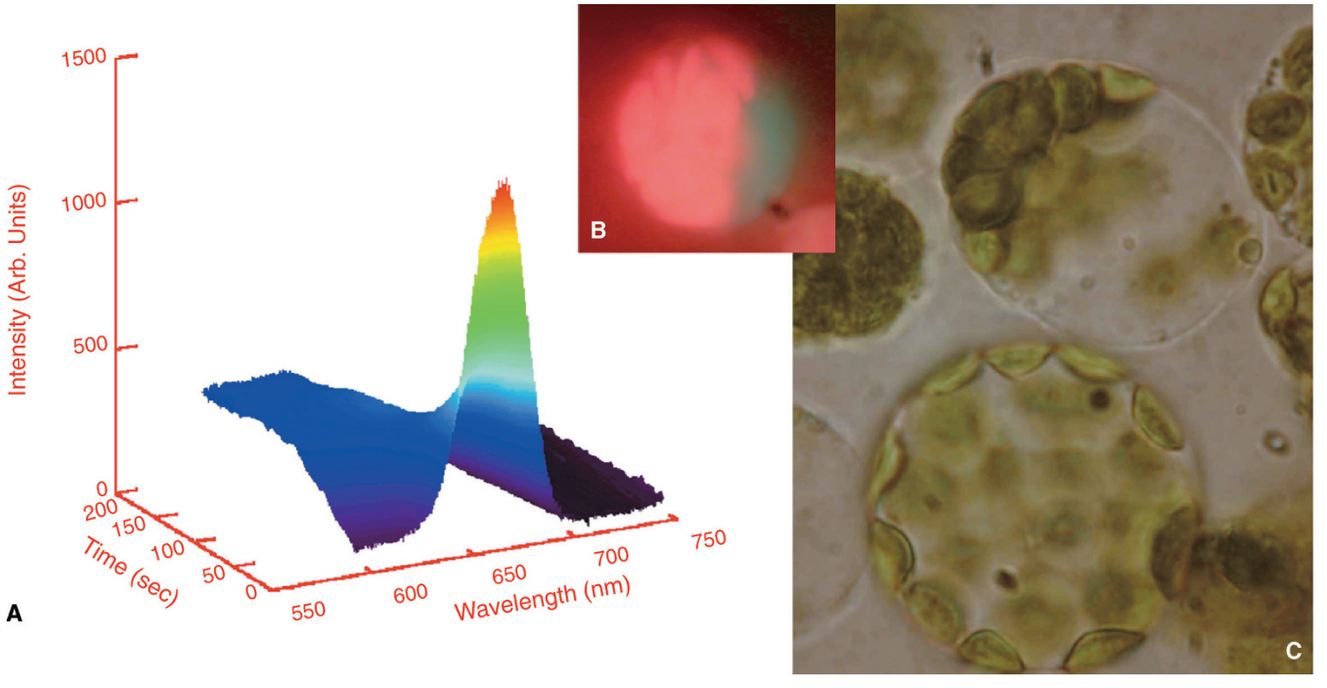

FIGURE 21.19. (A) Two-photon excited, time-lapse, microspectroscopy of maize (*Zea mays* L., Ohio 43) chloroplast in mesophyll protoplast, (B) conventional fluorescence micrograph of a maize protoplast, (C) conventional transmission micrograph of a maize protoplast.

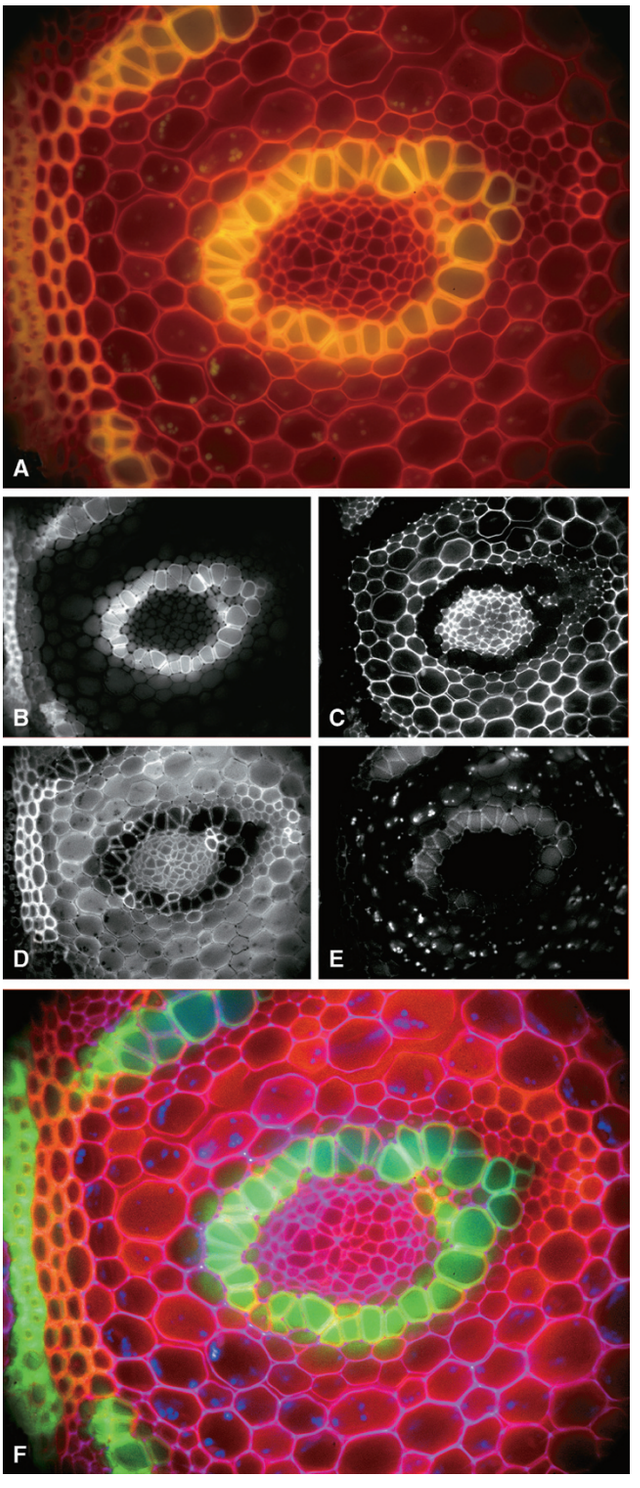

FIGURE 21.20. (A) Conventional fluorescence microscopy of the rhizome of lily-of-the-valley (*Convalaria majalis*). Classification of tissue structures based on their autofluorescence spectra, produced four images (B–E). (F) False color image of the combination of (B–E). Image obtained by using the Nuance Spectral Imaging System. (Images courtesy of Cambridge Research Instrument, Woburn, MA.)

overlapping autofluorescence. The *xy*-λ image was obtained by using a tunable, liquid-crystal (LC)–based, bandpass filter at 20 nm bandwidth and 30 nm steps. Different autofluorescence was chosen in various regions of the image, and spectral unmixing was performed on the image to remove the mixed autofluorescence. The technique clearly separates the fluorescence from parachyma cells from the Casparian band (Nuance Imaging System, Cambridge Research Instruments, Woburn, MA).

Light–Specimen Interaction (Fluorescence Emission)

Photoinduced damage can be characterized by a typical fluorescent intensity versus dose curve. Although usually the fluorescent intensity decreases as a function of exposure, this frequently does not apply to specimens of botanical origin. As plant cells generally, and particularly those capable of photosynthesis, are designed to capture and utilize light energy, light–specimen interactions often involve a series of pigment systems, and are much more complex than those observed in animal cells. On the other hand, as it is highly possible that fluorescence resonance energy transfer (FRET) occurs naturally in the photosynthetic system, introducing an exogenous donor–acceptor pair for a FRET study may be complicated by FRET from endogenous fluorophores in the plant cells. For example, one often notices an increase in chloroplast fluorescent intensity and a blue shift in autofluorescent spectrum upon illumination. Figure 21.21 shows the two-photon–excited fluorescence spectra of a protoplast culture versus exposure time. Note the initial increase in fluorescent intensity in the 630 nm chlorophyll peak.

Time-lapse, two-photon fluorescence microscopy (*xyt*) of the mesophyll protoplasts of *A. thaliana* yielded interesting results concerning cell viability under the high illumination intensity commonly used in multi-photon fluorescence microscopy. Upon NIR (760 nm) irradiation, the protoplasts emit blue-shifted fluorescence as shown in the two-channel, false-color image [combination of green (~500 nm) and red (~660 nm) channels]. In time-lapse studies, it was observed that the red fluorescence diminishes much more rapidly than the green fluorescence. This results in a blue shift of the fluorescence as a function of irradiation dose. Because

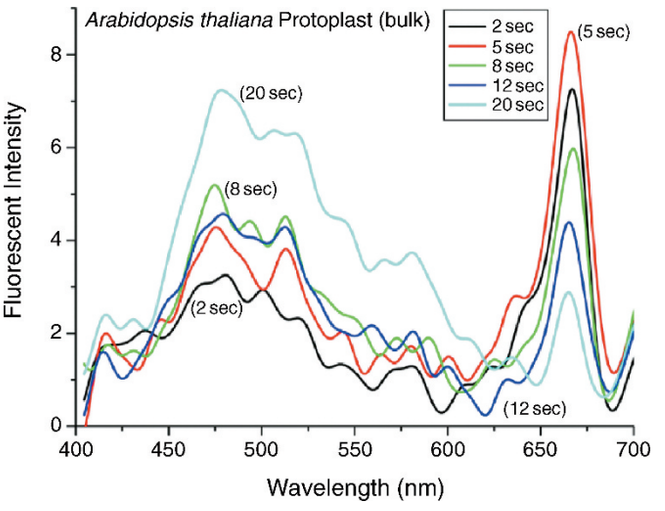

FIGURE 21.21. Two-photon fluorescence spectra of *Arabidopsis thaliana* protoplasts (in culture medium) versus exposure time. Note the red fluorescence intensity first increases before decreasing. Excitation, 760 nm.

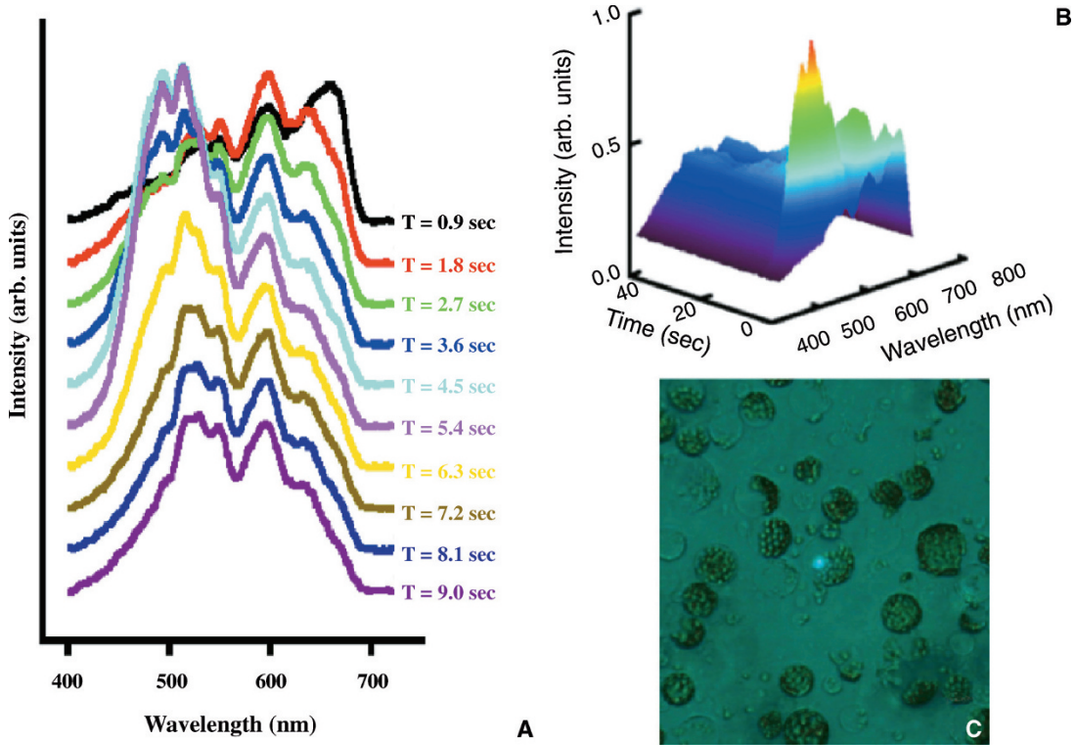

FIGURE 21.22. Two-photon time-lapse microspectroscopy of a single chloroplast (from *A. thaliana* mesophyll protoplast) showing complex spectral changes as a function of increasing exposure dose.

this rapid decrease in red fluorescence is accompanied by cellular uptake of neutral red/propidium iodide or the rapid loss of cytoplasmic-loaded Calcien dye (both of which indicate cellular damage), it might be possible to use the red-to-green fluorescence intensity ratio as an indicator of cell vitality (Cheng *et al.*, 2000a, 2001). This fluorescence study of protoplasts was confirmed by microspectroscopy of a single chloroplast, as shown in Figure 21.22. Figure 21.23 shows an area that received a single 3.3 s/frame scan (8.4 µs dwell time/pixel) at 768 × 512 pixels. As the total irradiated area is 180 µm × 120 µm and the average power was measured as 6.4 mW, the average energy striking each pixel is approximately 54 nJ (i.e., 8.4 µs at 6.4 mW). On the other hand, considering that the laser was operating at 82 MHz with 100 fs pulse with a numerical aperture (NA) 1.2 objective lens, the average and peak power densities at the focal point are approximately 3×10^6 W/cm^2 and 3.9×10^{11} W/cm^2, respectively. A significant reduction in red fluorescence is evident after such scans. Detailed analysis revealed that the red fluorescence, from chlorophyll-a and -b, initially increases slightly before decreasing. This initial increase is in agreement with the study of protoplast fluorescence in culture (Fig. 21.21), and is believed to be a physiological response to adjust the photosynthetic system to the high light intensity, perhaps involving the xenthophyll cycle.

As pointed out above, under high intensity illumination, cell survival can be monitored by the cytoplasmic retention of Calcein dye (loaded with Calcein-AM form; Molecular Probe Inc.) or by the entrance of neutral red/propidium iodide (cell death). It has been reported that multiple scans during image acquisition causes neutral red to enter the cells and/or Calcein dye to escape from them. These changes are then followed by visible structural damage such as shriveling or bursting of the cell. Figure 21.24 is a series of images obtained in sequence demonstrating cell damage under high intensity NIR illumination. Note the cell most heavily loaded with Calcein dye was damaged first (arrow). The high concentration of Calcein dye in the cell significantly increases the nonlinear absorption of NIR, causing more rapid damage.

It has been reported that, for a comparable red fluorescence signal level, single-photon excitation using 488 nm allows significantly more imaging scans before the cell begins to show photodamage (Cheng *et al.*, 2001a). Typical one-photon illumination power is in the order of 0.1 ~ 0.5 mW at the focal point (power density at 5×10^4 W/cm^2 ~ 2.5×10^5 W/cm^2), more than 6 orders of magnitude lower in power density than the peak power used in the two-photon imaging mode (3.9×10^{11} W/cm^2). Although two-photon fluorescence microscopy limits the photon-induced damage to the vicinity of the focal point, while in single-photon excitation damage is spread over the entire illuminated volume, many studies now show that, for the same signal level, high intensity, pulsed NIR illumination produces far greater damage to many living plant cells. This may be due to the fact that in a multi-photon excitation scheme, broadband absorption/excitation involving all the absorbers is possible, while in single-photon excitation, compounds only absorb energy if they have an absorption peak(s) at the excitation wavelength. It is important to point out that photo-induced damage occurs not only via the absorption/excitation of fluorescent molecules, but also because of absorption by any of the vast majority of non-fluorescing molecules.

When Schilders and Gu (2000) investigated the effect of multiple scattering in a turbid medium in single-photon and two-photon fluorescence microscopy, they demonstrated that

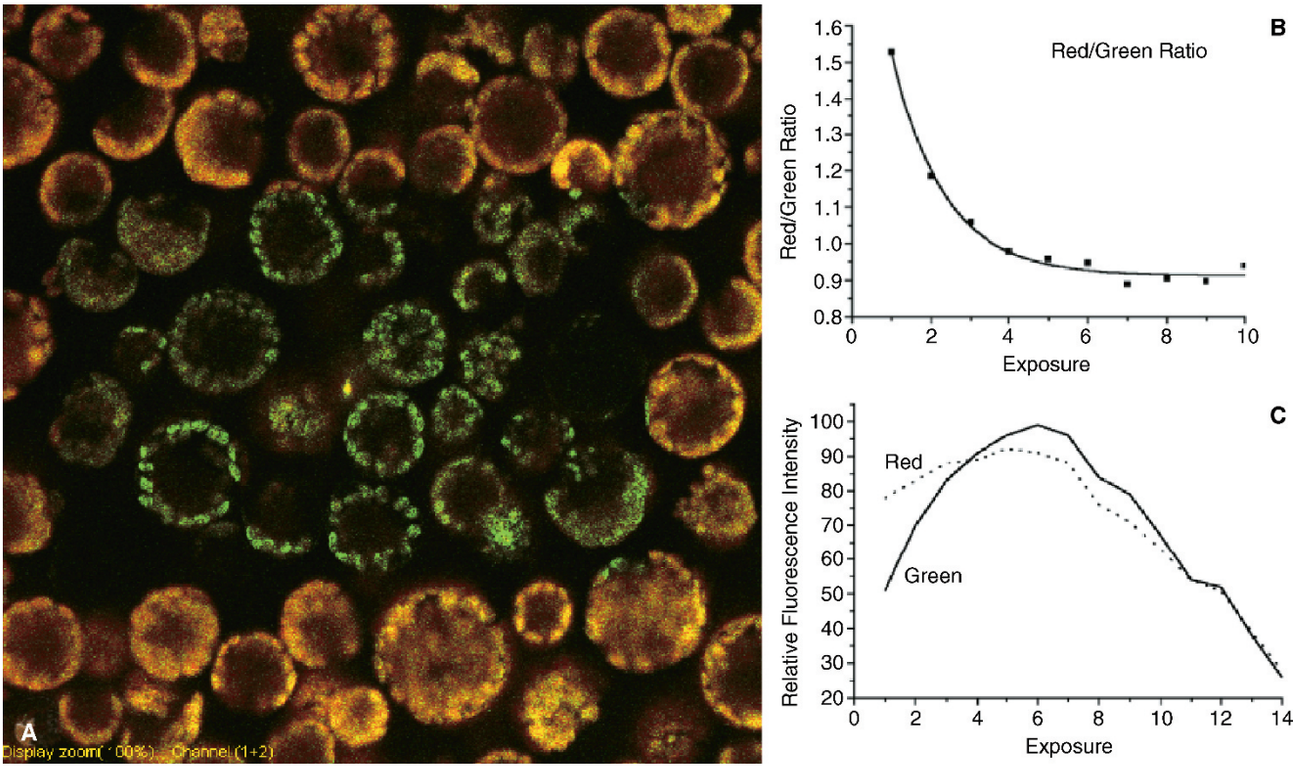

FIGURE 21.23. Two-photon fluorescence image of *A. thaliana* protoplasts. (A) The image was obtained by first scanning the central portion of the field (rectangular area) followed by a second scan to record a larger view. Note the single scan causes significant intensity and spectral changes in the autofluorescence (760 nm NIR excitation). (B) The ratio of the green and red channel intensity; (C) intensity variation plot of the green and red channels showing the initial increase in intensity.

two-photon excitation provides significant improvement in penetration depth in terms of resolution because the longer wavelength is scattered less. However, the two-photon image signal-to-noise (S/N) was appreciably degraded if a large fraction of the so-called ballistic photons in the excitation beam scattered. In addition, it was noted that the effective absorbance of a biological specimen in NIR (i.e., 800 nm) can be significantly higher at high illumination intensities because the nonlinear absorption coefficient increases with power level. Thus, the nonlinear absorption cross-section increases as the beam intensity increases towards the focal point and the effective opacity of the specimen can be much higher than the linear absorption measured at lower intensity (Fig. 21.5).

In two-photon fluorescence imaging, the achievable image quality is more often limited by low signal strength than by the optical resolution per se. In the case of the highly scattering *M. quadrifolia* leaf (Fig. 21.10), the optical sectioning depth is limited to approximately 40 to 50 µm. The two-photon image was obtained by using an Olympus Fluroview 300 confocal scanner and the flu-

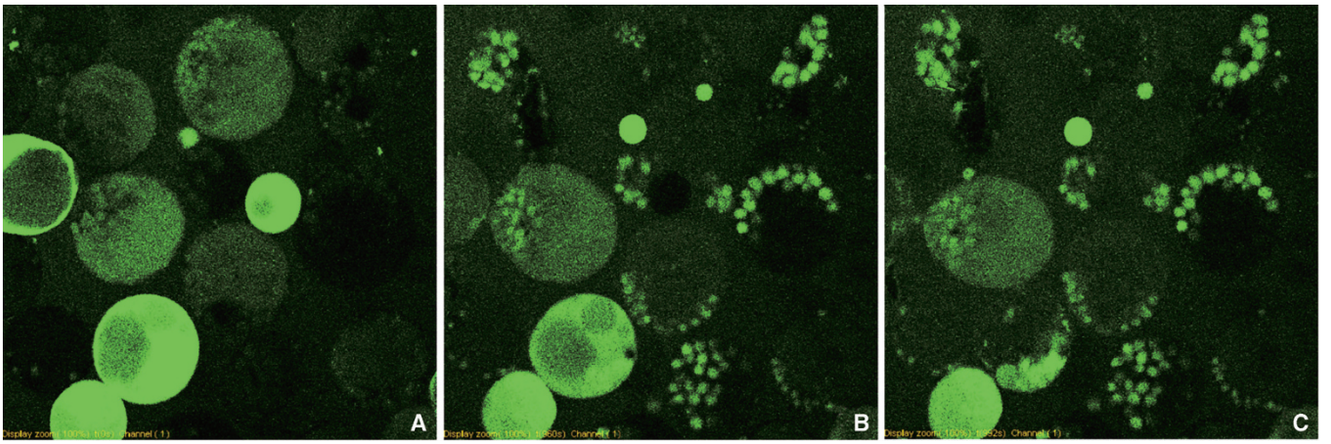

FIGURE 21.24. Series of two-photon fluorescence micrographs showing the photodamage of Calcein-loaded protoplast of *A. thaliana*. Note the cell most heavily loaded with dye is the first to be damaged (excitation, 760 nm; emission, 550 nm + 20 nm band; peak power density at focus is approximately 3.9×10^{11} W/cm^2 at 8.4 µs dwell time/pixel).

orescence signal was descanned and detected with the built-in photomultiplier tube (PMT) but no detector aperture was used. The fact that the two-photon excited fluorescence peaks are located near the attenuation maximum of this specimen further limits the detectable fluorescence. For comparison, the same specimen imaged in single-photon mode gave a usable depth of approximately 30 µm.

HARMONIC GENERATION PROPERTIES

A number of plant structures are capable of efficiently generating second harmonic signals. These include stacked membrane structures such as grana, starch granules, secondary cell wall, cuticle and cuticular waxes, and silica deposits (bio-opals). Starch granules exhibit high conversion efficiency in SHG, in fact, a piece of potato tuber placed in an unfocused, ultra-fast laser beam can efficiently generate a bright SHG beam in the forward direction (Fig. 40.10, *this volume*). Due to the radial symmetry of the molecular structure of a starch grain, starch granules exhibit birefringence, and it is believed that this molecular arrangement is also responsible for the SGH property. The efficiency varies with potato variety, presumably because of differences in the structure and size of the starch granules.

Cellulose is a linear molecule without branching. Neighboring cellulose chains may form hydrogen bonds leading to the formation of microfibrils (20 to 30 nm) with partially crystalline parts called micelles. This highly organized structure may be responsible for the strong SHG properties of cell walls. The term *biophotonic crystal* is used to describe biological structures having the physical properties required to generate harmonic signals (Sun *et al.*, 2001; Cheng *et al.*, 2003).

The SHG signal depends strongly on the polarization of the illumination beam. Figure 40.9 shows the rotation of SHG signal in maize silica cell as the polarization of the illumination changes. Because removing the organic matrix, using a $ZnCl_2$–HCl solution, destroys the SHG signal, it seems likely that it is the arrangement of the amorphous silica in the organic matrix that is important for SHG.

As the third harmonic signal is generated at optical interfaces, and as plant tissues are frequently highly heterogeneous in terms of refractive index, it is not surprising that many plant tissues generate strong THG. The surfaces of organelles, such as mitochondria and chloroplasts, lipid droplets, storage bodies (e.g., starch granules and protein bodies in seeds) and cell–wall interfaces are all capable of generating strong THG signals. Figure 21.25 shows a set of chloroplast images [THG (a), SHG (b), 2P-fluorescence (c), and combined image (e)] of mesophyll cells of *Commelina communis* L. obtained using 150 fs, 1230 nm illumination.

THE EFFECT OF FIXATION ON THE OPTICAL PROPERTIES OF PLANTS

When live-cell imaging is impractical or unnecessary, fixation by means of chemicals provides a way to avoid/minimize the problems with "uncleared" botanical specimens that are cataloged above.

While the primary purpose of the fixation process is to preserve the structure of interest, it may also be desirable to remove any constituents that might interfere with the observation. For example, alcohol-based fixatives (e.g., 1:3 EtOH/acetic acid; methanol, etc.) usually extract significant amounts of pigments from plant tissue, greatly reducing the autofluorescence background (Figs. 21.13, 21.14, and 21.15). These alcohol-based fixatives are commonly used to preserve protein structures. The use of a simple aldehyde fixative, such as formaldehyde, acroline, or 1:1:3 EtOH/formaldehyde/acetic acid mixtures, is also recommended.

As aldehyde fixation causes condensation reactions with tissue proteins that can result in ring formation and autofluorescence, it is normally avoided to prevent high background autofluorescence. However, Fredrickson used autofluorescence enhanced in this way, combined with excitation from the 488 nm Ar line to study the development of the female gametophyte in *Epipactis* (Fredrikson, 1992). Because glutaraldehyde, a di-aldehyde, can greatly increase background autofluorescence by forming excess crosslinkage of proteins, its usage should generally be avoided (for exception, see Chapter 18, *this volume*). The use of a fixative containing 1% freshly prepared para-formaldehyde and 1.5% acroline in 0.05 *M* phosphate buffer (pH 7.0) is recommended for its high penetration and excellent ultrastructural preservation (Cheng *et al.*, 1979b; use without the glutaraldehyde component). This fixative offers relatively low fixative-induced, autofluorescence and offers the possibility of both SEM and TEM studies after optical observations (see Chapter 49, *this volume*). The brownish coloration of plant tissue caused by natural tannins or the oxidized products of fixation can be removed by the treatment in Stockwell's solution for 10 to 20 h (Johansen, 1940; Herr, 1985, 1992; Palser *et al.*, 1989).

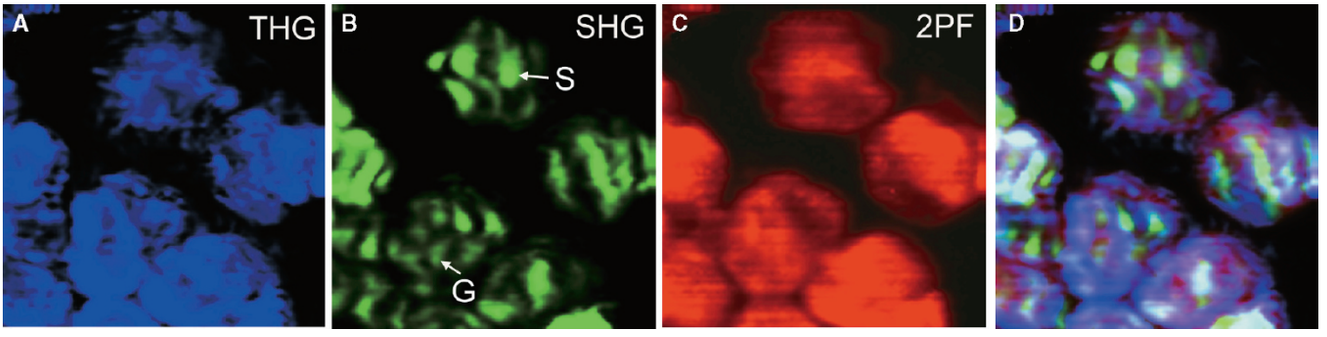

FIGURE 21.25. SHG, THG, and two-photon fluorescence image of chloroplast. (A) The THG signal is generated at the interfaces of refractive index while the SHG signal (B) is generated by the stacked membranes in the grana (G) and by the starch granules (S). The 2P-fluorescence (2PF) signal is the result of chloroplast autofluorescence. Panel (D) combines images of (A), (B), and (C).

LIVING PLANT CELLS

As it is not possible to modify the optical properties of a living plant cell, one can only optimize the imaging method to achieve best attainable images. These methods include the selection of the proper excitation wavelength(s), a suitable detecting wavelength (if possible), a suitable water-immersion or dipping objective and the choice of single- or multi-photon excitation. In addition, imaging modalities such as BSL imaging or SHG should be considered as these methods do not deposit any energy in the specimen. Spectral imaging may help to separate the emission from the fluorescent tag(s) from that caused by autofluorescence.

Unlike many common cultured animal cells, neither suspension-cultured plant cells nor free-living algae attach to culture dishes or to any other substrates. As a result, immobilizing suspending cells can become a challenge. Most of the discussion so far in this chapter has been focused on the photosynthetic tissues. The following sections will discuss the technical issues specific to imaging particular organs and tissues.

Callus, Suspension Culture Cells and Protoplasts

Parenchymal tissues can be cultured in suitable artificial media. The cells remain in an undifferentiated state and form aggregates called callus. The callus remains colorless when kept in the dark, but generally turns green under light. Therefore, depending on the type of callus, one may encounter different levels of autofluorescence background. Imaging GFP, yellow fluorescent protein (YFP), and DsRed is relatively easy in a colorless callus, but spectral overlap will occur in green callus. In order to improve the optical properties of the specimen, it is important to mount the callus under a coverslip and in a suitable culture medium, so that there is no air interface between the water-immersion objective lens and the callus.

Suspension-Cultured Cells

Suspension-cultured cells are relatively easy to image because most of them develop only the primary cell wall. However, immobilizing suspension cells requires some effort. Methyl-cellulose, agrose (0.5%–1%) and polyvinyl alcohol gel (such as K-Y Jelly) can be used to immobilize such cells in a chambered slide [Fig. 21.26(A)]. Cells can also be held in a specially designed chamber

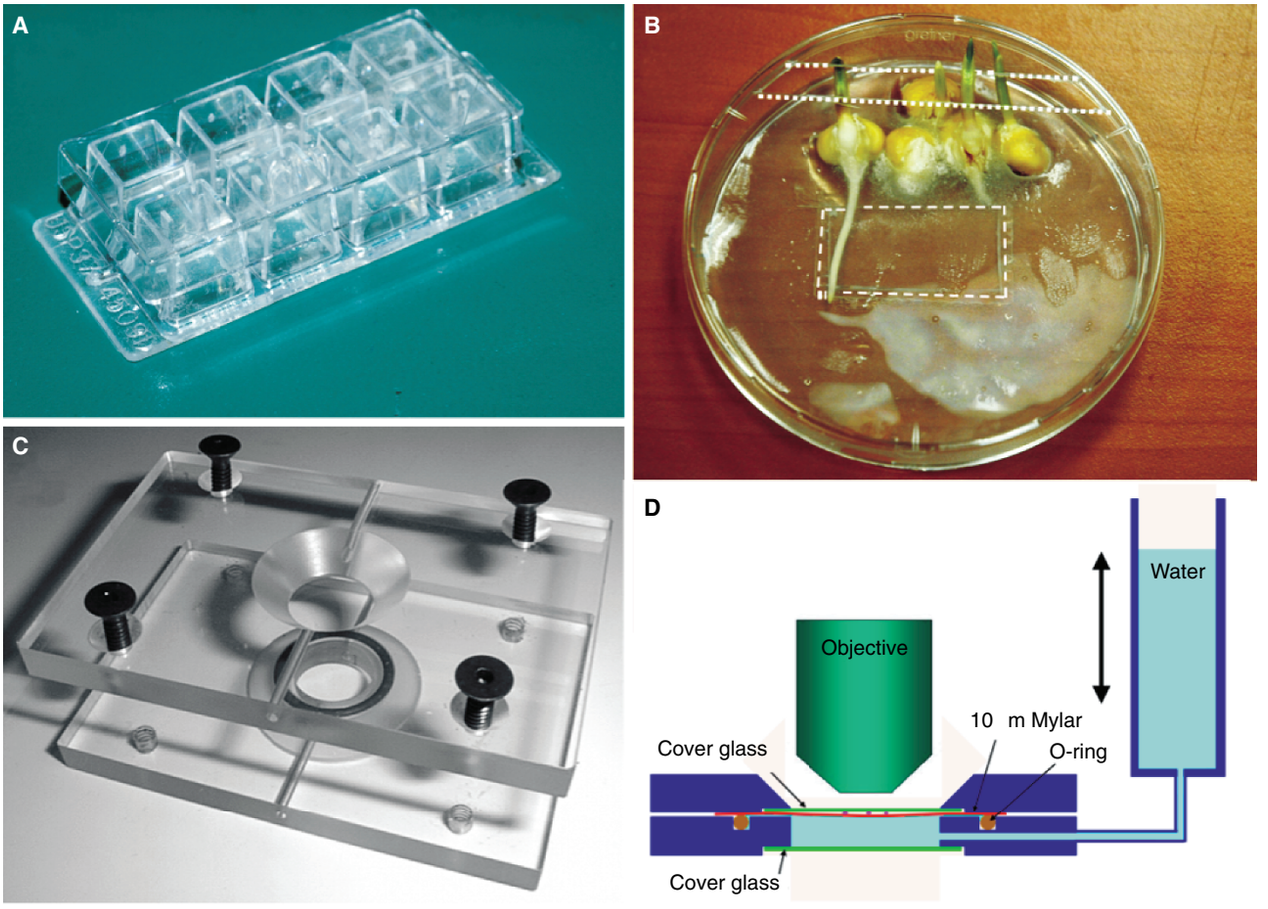

FIGURE 21.26. (A) Chamber slides commonly used in handling cultured plant cells. (B) A homemade, larger version of the chambered slide, filled with agrose gel, can be used to observe the roots of small plants — note the opening in the upper lid to allow plants to grow and the bottom of the Petri dish (*dotted rectangular area*) has a window made of a coverslip having the proper thickness. (C) A specimen chamber designed to handle loose tissue or cultured cells; (D) diagrammatic representation of the chamber shown in (C). The chamber is made of an upper and a lower cover glass window (green) with a 10 µm Mylar film (red) located just below the upper coverslip. Cells or loose tissues are held between the upper coverslip and a Mylar film. The lower chamber is filled with water and connected to a water reservoir via a flexible tube. The amount of "holding" pressure exerted on the specimen by the Mylar film can be adjusted by the height of the water head (Cheng *et al*., 1999a). (Other chambers are discussed in Chapter 19, *this volume*)

such as that shown in Figure 21.26(B) (Cheng *et al.*, 1999a). Figure 21.27 shows GFP-expressing tobacco cells held in a chamber slide with 0.5% agrose gel. Through-focus series of fluorescence images were obtained at video rate using the widefield, epi-fluorescence mode and subsequent deconvolved (AutoDeburr, AutoQuant Inc., Troy, NY) to obtain optical sections. Success in this technique requires that the specimen be immobile during the entire data collection process.

Protoplasts are plant cells that have had their cell walls removed by enzymatic digestion. When suspended in liquid medium, they are generally spherical in shape and can be imaged using the same methods as for suspension cells. If the protoplast is derived from a mesophyll cell, it may contain large numbers of chloroplasts as shown in Figure 21.28. The image shows the red autofluorescing chloroplasts and green fluorescing mitochondria in a mesophyll protoplast of *A. thaliana*. The cell was labelled with Mitotracker (Molecular Probes Inc.) in culture medium (Huang and Chen, 1988).

Calcein AM dye (Molecular Probes Inc.) provides a good measure of plant cell and protoplast viability. The AM–ester salt can be loaded into the protoplast. After incubation, wash with fresh medium and mount in a chamber slide. Lower concentrations of dye may be necessary as excess dye loading can greatly increase the linear and nonlinear opacity of the cell. This results in a significant increase in energy deposition by the illumination and can pose a serious problem in confocal or multi-photon fluorescence microscopy. Figure 21.24 shows a series of images taken from Calcein AM-loaded protoplasts (leaf of *Zea mays* L.). Note the rapid cellular damage in the cells most heavily loaded with dye.

Meristem

The apical meristem is the site of the tip growth that is one of the most striking features of plant growth. Although meristems potentially have an unlimited ability to divide, division is controlled and regulated resulting in the proper initiation of leaves and suppression of the development of lateral buds (apical dominance). Confocal microscopy and multi-photon fluorescence microscopy is well suited for the study of leaf and floral initiation in the meristem. Backscattered light mode can be used to perform time-lapse imaging on the transformation of vegetative to reproductive growth in the apical meristem. On the other hand, multi-photon fluorescence microscopy can be used to image cell organization and division orientation in an initiating leaf primordium (Bommineni *et al.*, 1990, 1993, 1995). Figure 21.29 is a BSL image of a maize apical meristem.

Stem and Root

In the stem and root, vasculature is the most frequently studied tissue. The vascular bundle consists of the elements of water conduction, the xylem, and those of assimilate conduction, the phloem. The phloem is the principal food-conducting tissue in vascular plants. Mature phloem elements are called sieve tubes. At regular intervals callose is deposited to form sieve plates between sieve-tube members and these can be detected with Resorcin blue. Decolorized aniline blue (pH 10) can be used for staining both fresh sieve tubes and those fixed in EtOH–acetic acid (3 : 1). The amount of callose increases as the cell ages, and this continuously reduces the diameter of the pores. Because increased callose formation

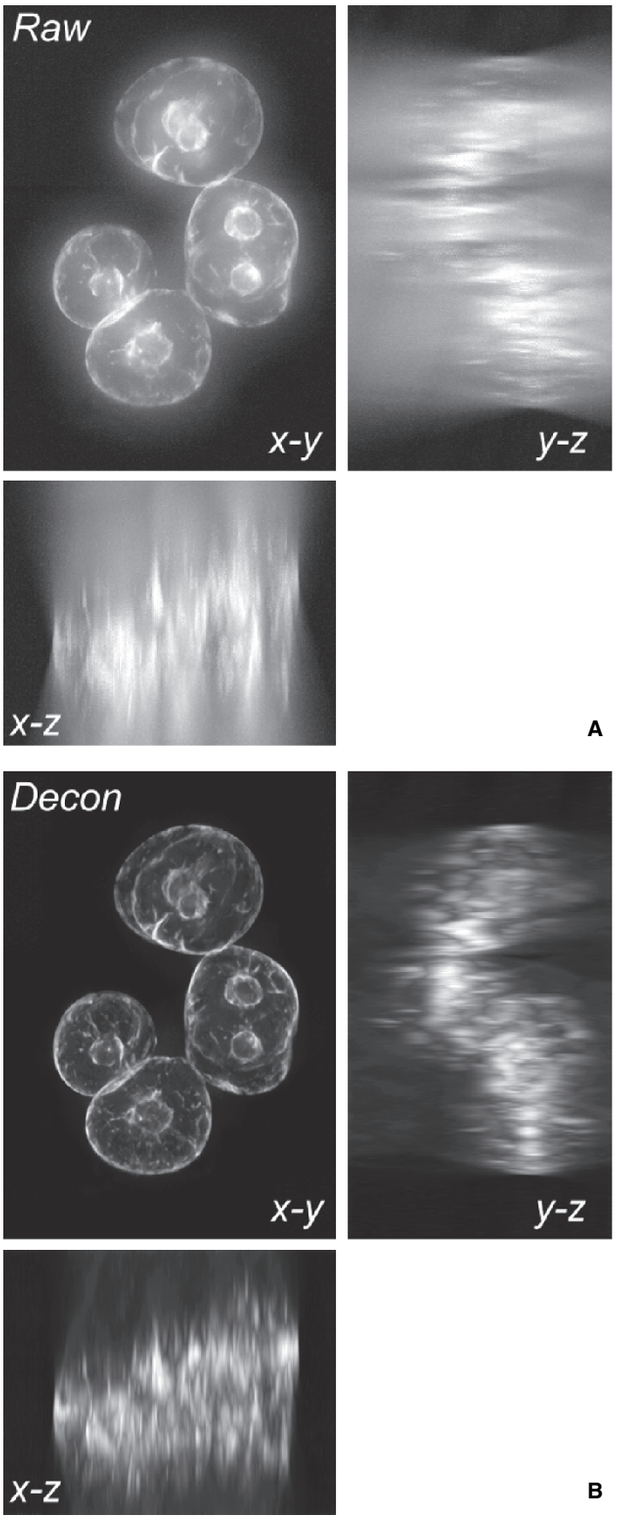

FIGURE 21.27. Widefield fluorescence microscopy of suspension-cultured GFP-tobacco cells. (A) Projection of a series of widefield, epi-fluorescence, through-focus images (*xy*, *xz*, and *yz* views). (B) Projection of a deconvolved image stack from (A). Fluorescence images were obtained with blue excitation and recorded as 550 nm emission. Image was recorded with a low cost video-rate CCD camera using ImageAcquire acquisition software (Ming-mei Technology Inc., Taipei). Deconvolution was performed using AutoDeblur v.9.3 (AutoQuant Inc.). (Image obtained at the 2002 International Course on Live Cell Imaging held at the University of British Columbia, Vancouver, Canada.)

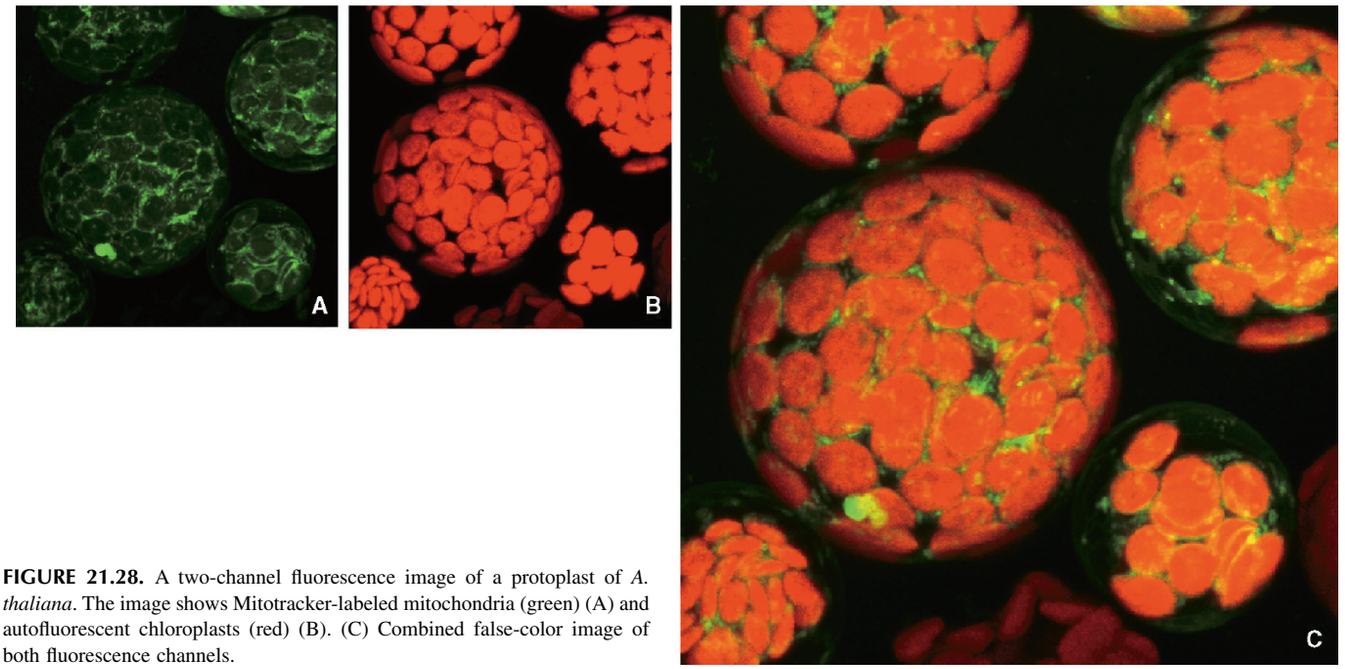

FIGURE 21.28. A two-channel fluorescence image of a protoplast of *A. thaliana*. The image shows Mitotracker-labeled mitochondria (green) (A) and autofluorescent chloroplasts (red) (B). (C) Combined false-color image of both fluorescence channels.

occurs in response to injury or infection, this staining method can also be used in pathological studies of plant tissue. In addition, callose can also be stained by the use of Cellufluor. The Casparian band in root can be stained by berberin hemisulphate/aniline-blue (Brundrett *et al.*, 1990; Hose *et al.*, 2001).

One of the common features of vascular plants is their ability to synthesize lignin. This substance is deposited in the cell walls of lignified tissue, particularly the xylem, to provide rigidity to the otherwise elastic polysaccharide cell walls. Lignin is a high-molecular-weight polymer of substituted cinnamyl alcohols that contributes about 20% to 30% of the dry weight in woody stems. It gives strong autofluorescence when excited by ultraviolet (UV)/blue light or by multi-photon NIR. These autofluorescence properties can be used to study vascular bundles or secondary wall thickenings. Woody root tissues that contain so much of lignin and alkaloids produce such intense autofluorescence that it is generally difficult to image exogenous dyes in them, although the fluorescence emission can sometimes be separated using spectral unmixing (Fig. 21.20).

Synchronous mitosis can be achieved in plant tissue by the use of colchicine or hydroxyurea (Carvalho *et al.*, 2002). This technique is commonly used in the treatment of root tips to obtain a high number of mitotic figures. Polarization microscopy can be used in the study of the dynamics of mitotic spindles consisting of birefringent microtubules.

Mounting Roots for Imaging

The glass-bottomed Petri dish shown in Figure 21.26(B) can be used in the study of root tips and root hairs. A rectangular hole was cut at the bottom of the Petri dish and a coverslip was glued over it with SilGaurd. Then, 0.5% to 2% agrose gel was pipetted into the dish and allowed to set. Seeds can be set on the surface or embedded in agrose in one side of the dish so that the seed can germinate while the dish is placed horizontally. As soon as the young roots reach the bottom of the dish, place the petri dish at a 45° to 60° angle on a stand, to force the root to grow downwards along the surface of the cover glass. This method minimizes the distance of root tissue from the coverslip, creating good optical conditions for microscopy. The root portion of the dish should be kept in the dark and an opening in the cover may be needed to allow the seedlings to emerge. Smaller plants, such as *Arabidopsis*, can be seeded in a small-chambered glass [Lab-Tek; Fig. 21.26(A)]. An inoculation of a fungal plant pathogen can be applied to the agrose after germination and pathogen–root interactions can be studied through the coverslip window at the bottom of the Petri dish. Figure 21.30 is a fluorescence confocal image of the root tip of maize.

Microspores and Pollen Grains

Microsporogenesis can be imaged either by isolating the microspore from an anther or by studying a whole-mount specimen. Isolated pollen mother cells or microspores can be handled the same way as suspension-cultured cells. However, it is frequently desirable to image the microspores *in situ* (Pace *et al.*, 1987) through the anther wall. Multi-photon fluorescence microscopy is the choice for this application. Because high resolution is generally needed to study this type of specimen (i.e., chromosomes, microtubules, etc.), special care should be taken to ensure that the optical properties are matched as closely as possible to the design criteria of the objective lens. If the tissue can be fixed, stained, and cleared in methyl-salicylate, it can produce exceptional images (Cheng *et al.*, 1999b; Fig. 21.31). In addition, it can be helpful to apply adaptive deconvolution [i.e., "blind" deconvolution, capable of finding the best-fit PSF for 3D multi-photon or confocal data stacks (see Chapter 24, *this volume*)]. The three-dimensional chromosomal arrangement can also be obtained by using widefield epi-fluorescence microscopy and deconvolution (Agard and Sedat, 1983; Agard *et al.*, 1989; Dawe *et al.*, 1992); the technique is particularly attractive when DAPI (Vergne *et al.*, 1987) is used for staining of the chromosomes because UV excitation is readily available in conventional epi-fluorescence.

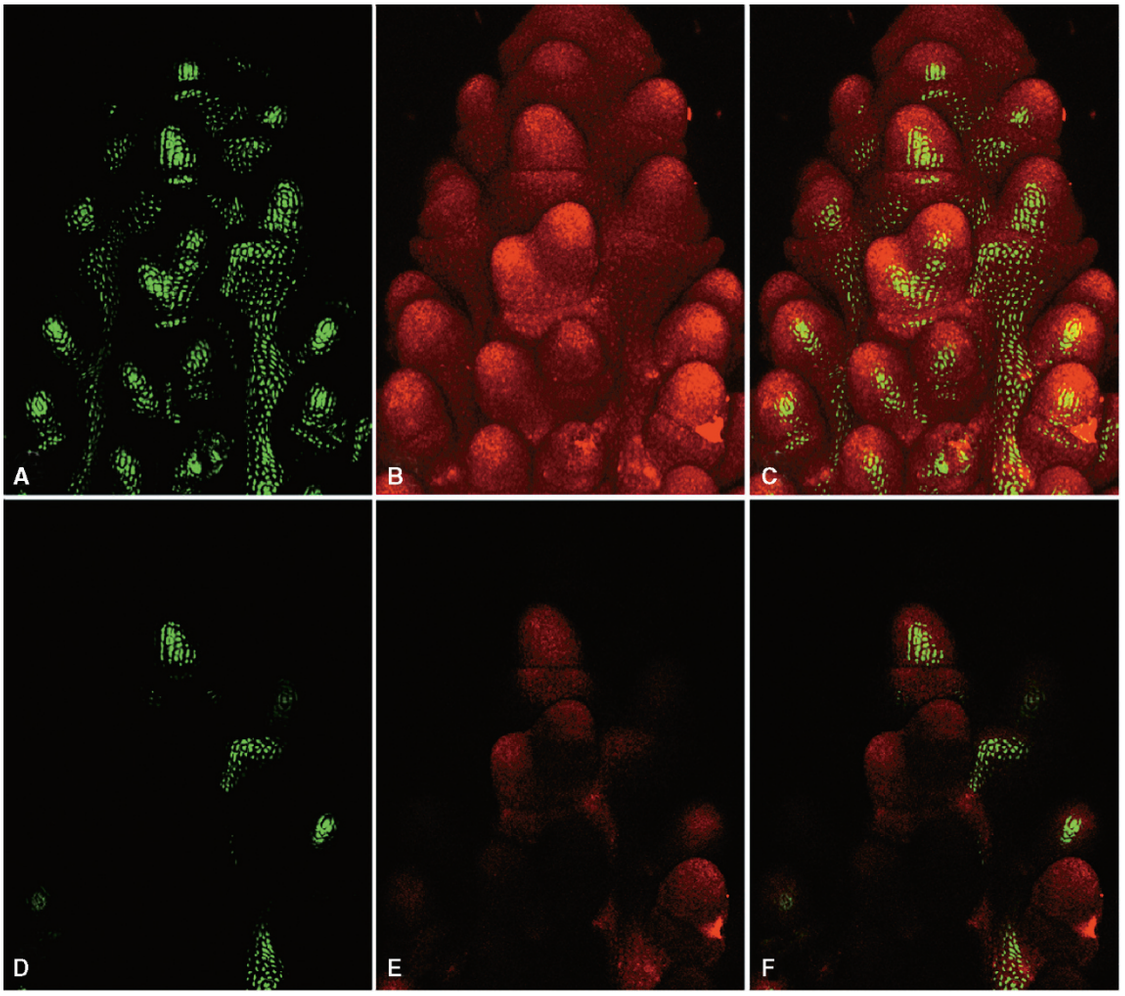

FIGURE 21.29. Confocal image of the apical meristem of maize.

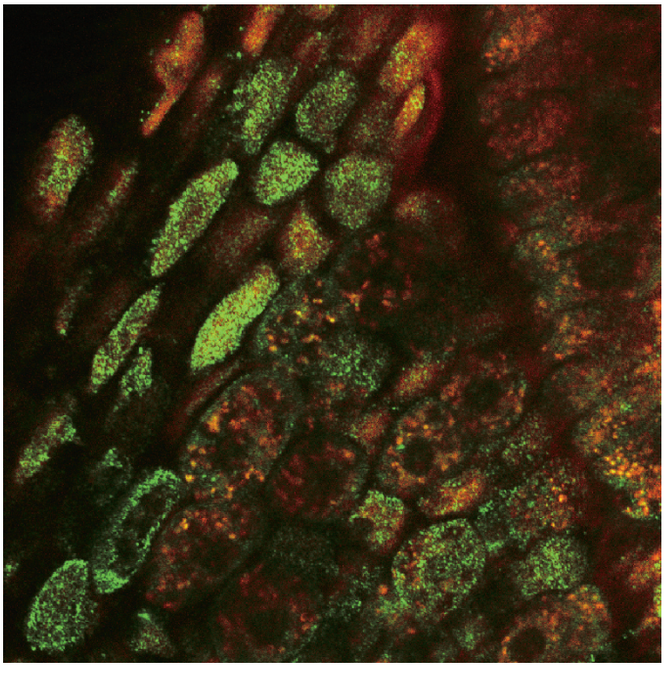

FIGURE 21.30. Two-channel confocal image of root apex of maize.

Because microtubules are birefringent structures, the spindle in the dividing cells can also be imaged by dynamic polarization microscopy (e.g., Spindleview from Cambridge Research Instruments, Woburn, MA). However, as the anther wall can also be highly birefringent, it may be better to image isolated pollen mother cells.

Pollen Grains

Pollen grains are difficult specimens to image as they are frequently both highly scattering and pigmented. The surface of the pollen grain is covered with a sporopollenin exine and a cellulose intine (Heslop-Harrison and Dickinson, 1969). The exine consists of complex fine structures that make the pollen grain not only a highly absorbing but also a highly scattering specimen. Because pollen grains also frequently contain a large number of starch granules and a relatively dense cytoplasm, significant self-shadowing can occur when imaging them. Figure 21.32(A) shows the autofluorescence spectra of maize pollen. As it is clear that this autofluorescence background is high for almost the entire visible spectrum, when studying pollen grains, consider fluorescent dyes that emit in the NIR. The autofluorescent signal can be excited by UV, blue light or multi-photon of NIR. Figure 21.32(B,C) shows a pollen tube (PT) penetrating the hair (hr) of silk (S). Note the high autofluorescence of the pollen grain (P). Other pollen images can be found in Figures 8.49 and 8.60.

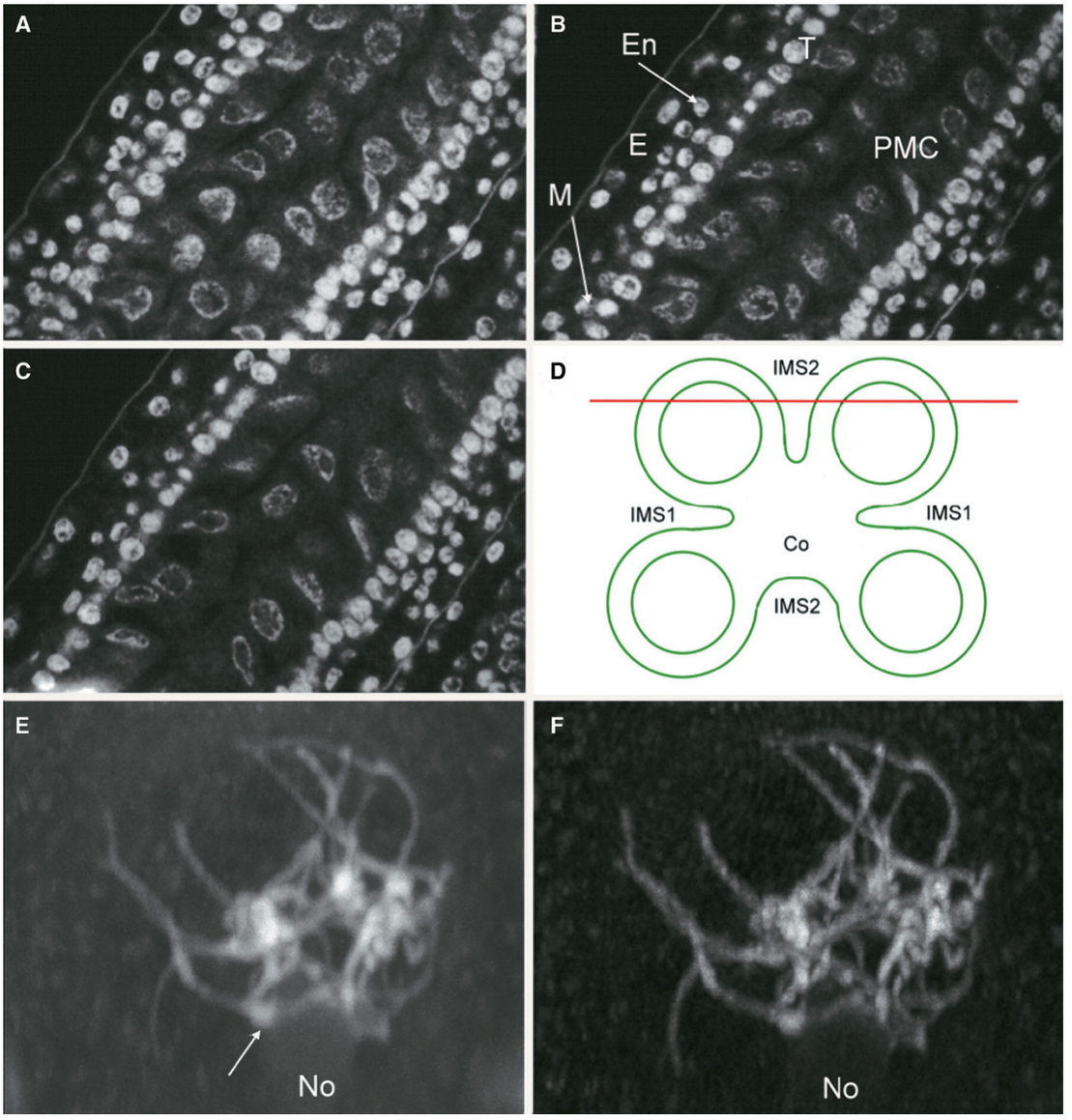

FIGURE 21.31. (A) Meiosis of maize pollen mother cell. (A, B, C) Representative images from an optical section stack of maize anther. (D) Approximate position where the optical sections were obtained from the maize anther. (E) Pachytene chromosomes in the pollen mother cell (PMC); this image was obtained directly through the four-layer anther wall using a confocal microscope (excitation, 514 nm; emission, 600 nm). (D) Deconvolved image of (E). Specimen was stained with Feulgen reaction and cleared in methyl salicylate. IMS1 and IMS2 are intermicrosporangial stripe 1 and 2, respectively. Co, anther connective; E, epidermal cell; En, endothecium; M, middle layer; T, tapetum; No, nucleolus.

Tapetum

The tapetum film and the orbicule [Ubish body, Fig. 21.32(D)] are also made of sporopollenin (a polyester of several monomers of which beta-carotene and zeaxanthin are the most common) and have the same autofluorescence properties as pollen exine (Echlin and Godwin, 1968; Dickinson and Bell, 1972; Cheng *et al.*, 2004) that produces intense autofluorescence [Fig. 21.32(E)]. Therefore, because studying tapetum development after the young microspore stage (onset of sporopollenin deposition) may suffer from high background autofluorescence, it may help to use fluorescent probes excited in deep red or even NIR.

Starch Granules

As stated above, starch granules are efficient SHG producers. Therefore, when imaging pollen with a multi-photon fluorescence microscope, it is highly possible that the scattered SHG signal can significantly contaminate the recorded fluorescence signal. In this case, it is wise to check the fluorescence spectrum to ensure that SHG signal is not present. Alternatively, one can place a long-pass barrier filter to remove the SHG signal from the fluorescence-detecting path. This SHG light can also excite additional autofluorescence.

Pollen Germination

Although it is common to image pollen germination on the surface of an agrose gel, imaging the penetration of a pollen tube into a style can be more challenging. In order to optically match the design criteria of a "non-dipping" water-immersion objective lens, it is essential that a coverslip with proper thickness be added on top of the agrose gel. A small spacer may be needed in between

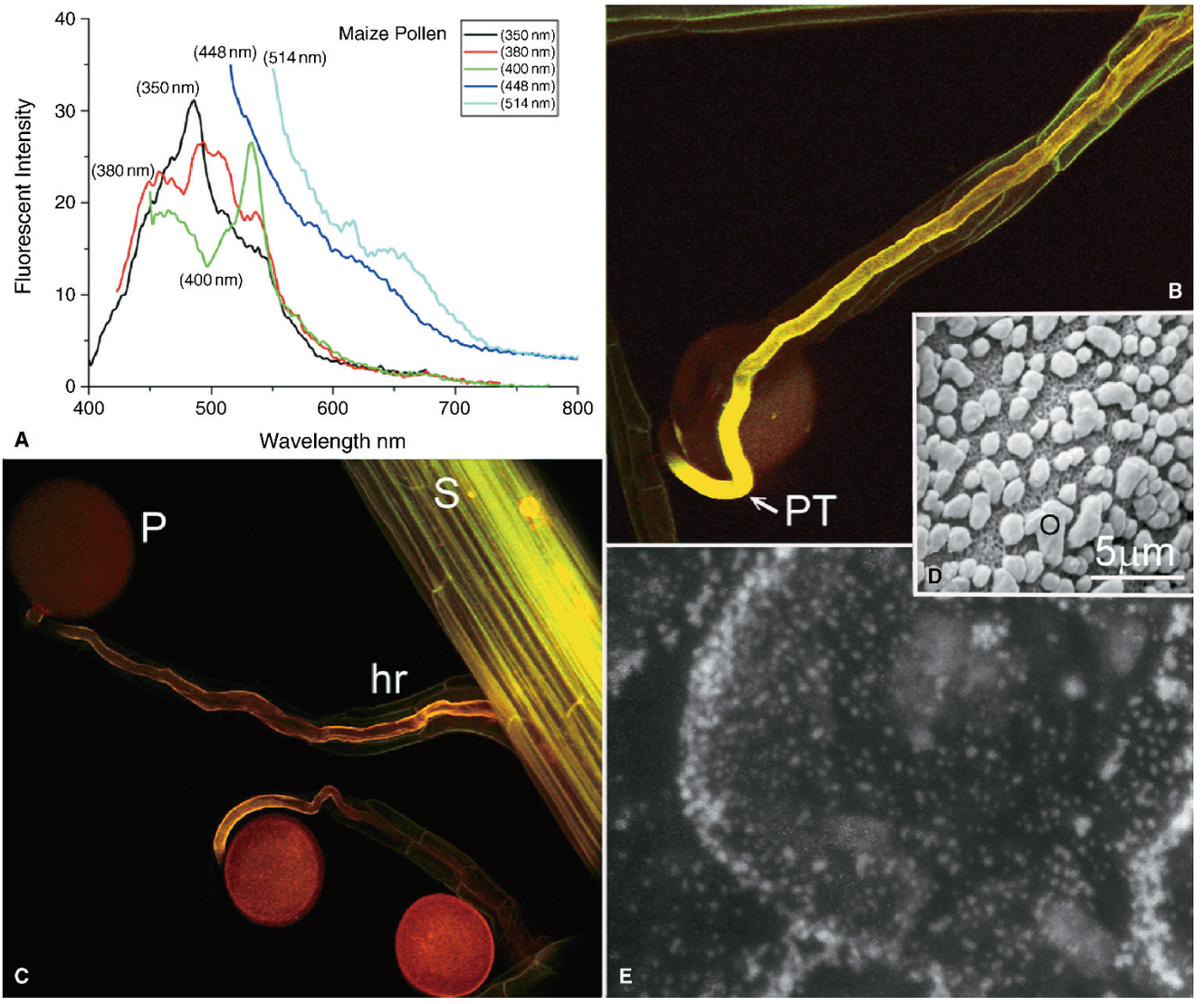

FIGURE 21.32. (A) Single-photon–excited fluorescence spectra of maize pollen grains (*Zea mays* L., var. KYS). The spectra were obtained by exciting pollen grains with 350 nm, 380 nm, 400 nm, 448 nm, and 514 nm. Note the strong autofluorescence in the blue and green regions when excited with UV and deep blue light (350, 380, and 400 nm), and significant red fluorescence when excited with blue and green light (448 and 514 nm). (B and C) Single-photon, two-channel fluorescence image of germinating pollen grain (P) on the hair (hr) of the silk (S). Note the penetrating pollen tube (PT). (D) SEM image of isolated tapetum film with orbicules (O). (E): (Style) autofluorescence image of orbicules in maize (excitation, 488 nm; emission, 610 nm).

the agrose gel and the coverslip to prevent it crashing into the germinating pollen grain. Decolorized aniline blue (pH 10) can be used for staining both EtOH–acetic acid (3 : 1) fixed and fresh callosic inner wall of the pollen tube (Pareddy *et al.*, 1989).

Rapid cytoplasmic streaming within the pollen tube usually requires high-speed imaging devices such as the disk-scanning confocal microscope (for more about fast confocal imaging see Chapter 10, *this volume*). High-speed, ratiometric imaging also allows the study of Ca^{++} gradients at the tip of the pollen tube using Ca^{++} sensitive dyes (see Chapter 42, *this volume*). Figure 21.33 shows a Ca^{++} ratiometric image of the tip of lily pollen tube, imaged by a confocal microscopy using the Fluo-3/Fura Red scheme.

Cuticles, Hairs, and Waxes

The outer surfaces of terrestrial plants are generally covered with an inert polymer of cutin and waxes (Cheng *et al.*, 1981, 1986; Cutler *et al.*, 1982; Juniper and Jeffree, 1983; Cheng and Walden, 2005). The most common constituents of the cuticle are 9,10,18-trihydroxyoctadecanoic acid and 19,16-dihydroxyhexadecanoic acid (Holloway, 1982). The reactive groups of these molecules link and crosslink into a high-molecular-weight, three-dimensional network. There is usually an excess of free hydroxyl (–OH) and carboxyl (–COOH) groups that can be stained with basic dyes. In some cases, such as that of tomato fruit, the cuticle is pigmented with carotinoids and shows strong autofluorescence. Cuticle can also be stained by the fluorescent dye berberin sulphate. The reverse (or "negative") fluorescence method can also be used to study the surface topography of a cuticle layer, such as the ridged cuticle found on the anther surface of maize (Cheng *et al.*, 1986).

Terrestrial plants frequently have additional wax covering the surface of the cuticle. These waxes can be laid down in complex structures (plates, needles, etc.) and can be highly birefringent. Plant surface waxes are complex chemical mixtures composed

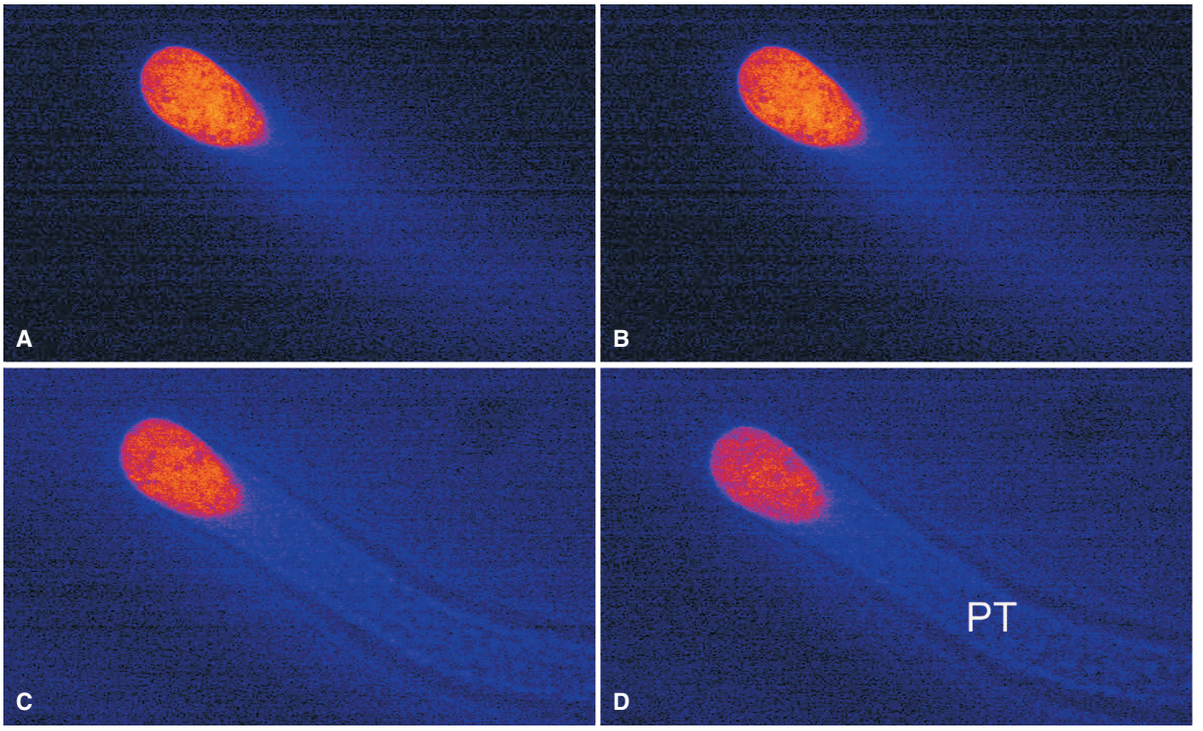

FIGURE 21.33. Ca^{++} ratiometric image (serial optical sections) of the tip of lily pollen tube (PT). (Image obtained at the 2002 International Course on Live Cell Imaging held at the University of British Columbia, Vancouver, Canada.)

mainly of long-chain aliphatic hydrocarbons with chain lengths ranging from C_{20} to C_{35} (Bianchi and Salamini, 1975; Bianchi *et al.*, 1977, 1978; Tulloch, 1981; Baker, 1982; Blaker 1989; Cheng *et al.*, 1986). These waxes can form complex surface structures and are difficult to study morphologically because of their sensitivity to electron beam irradiation in a scanning electron microscope. The waxy surface structures can be studied by using a confocal microscope with either BSL imaging or reverse contrast fluorescence in which the surface is wetted by the fluorescent solution.[1]

The air–cuticle–water interfaces are optical interfaces between RI = 1/1.4/1.3. This difference is high enough to effectively lower the solid-angle of high-NA objectives. The air–cuticle–water interfaces can also generate THG signal when illuminated at high intensity. Trichomes and hairs are additional strongly-scattering structures on the surfaces of many plants. To reduce the deleterious optical effects of these structures, it is wise to mount such plant tissues in water or, if possible, in RI-matching glycerol/water solution. This measure reduces the RI difference between the medium and the epidermal surface (wax and cuticle) from 1.0/1.4 (air/cuticle) to 1.3/1.4 (water/cuticle). However, if one is trying to image the organ surface (i.e., the surface of the leaf), an air/tissue interface is desirable as it can easily be imaged using BSL. This imaging modality allows researchers to monitor the development of an organ or tissue over a long period of time using low light intensity and without adding fluorescent dyes. Cuticle can also be separated from the cell wall and studied in this way (Holloway and Baker, 1968). Figure 21.34 shows extended-focus images of the surface of the leaf by BSL mode (green) and underlying cells in fluorescence mode (red).

[1] To ensure low staining of the waxy structures, it is important to use dyes that have a low partition coefficient in waxes.

Storage Structures

Starch granules, protein bodies, and lipid granules are commonly found in plant cells. In most cases, if the density of these granules is relatively low, no significant influence on the signal strength will be detected. However, in tissues where a large number of storage granules is present (endosperm cells, pollen grains, and other storage cells), significant deterioration both in image quality and signal strength should be expected. This is particularly serious when the granules are stained with dyes that have strong absorption characteristics in the excitation and/or emission wavelengths.

Oils found in plant cells commonly have refractive indices higher than that of water. For example, most of the commercially used plant oils have refractive indices in the range of 1.4 (Lide, 1991). Therefore, these substances can generally be imaged in the BSL mode as well as by using fluorescent dyes such as Neutral Red (Kirk, 1970) or Nile Red. The fluorescence excitation and emission maxima of these dyes may vary, depending on the hydrophobicity of the environment. Nile Red can be used at a concentration of 100 ng/mL, and can be excited with the 488 nm/514 nm Ar-ion lines, with emission detected using a 530 nm/590 nm longpass. Figure 21.35 shows the lipid and protein storage granules of maize endosperm imaged by two-channel fluorescence confocal microscopy. Note the dense tissue resulting in very shallow penetration.

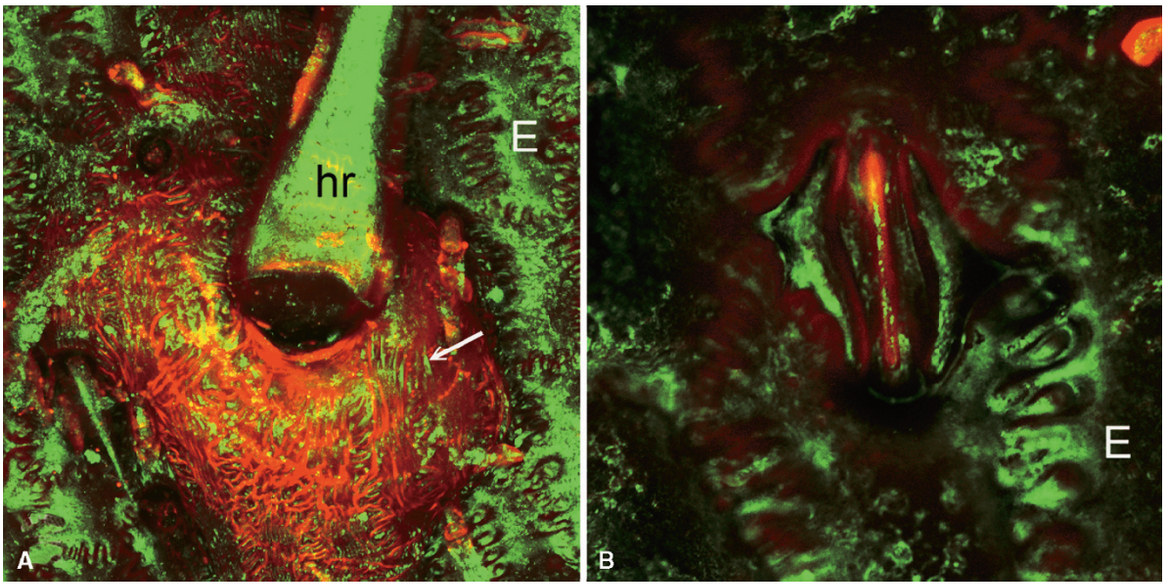

FIGURE 21.34. Extended-focus image of the leaf surface of maize. (A) Ridged cuticle (*arrow*) can be found at the base of a hair (hr); the surface of the interlocking epidermal cells (E) is clearly visible. (B) Stomata and interlocking epidermal cells. Note that the secondary wall of the guard cells produces intense autofluorescence. Green, backscattered light signal; red, autofluorescence signal.

Mineral Deposits

Mineral deposits are frequently found in and around cells in plants. For example, SiO_2 deposits are common in specialized cells and in the cell wall of the epidermal cells of grasses (Dayanandan *et al.*, 1983; Hodson and Sangster, 1988; Cheng *et al.*, 1990; Kim *et al.*, 1990) and *Equisetum*. The SiO_2 deposition is amorphous in nature and commonly referred to as biological opal. Bio-opals have an RI of around 1.42. As this is significantly different from that of the surrounding aqueous medium, it produces a strong BSL signal. The surface of these deposits can be rough (on the hundreds of nanometer scale) and they often have many internal lacunae from a remnant of cytoplasmic strands. Figure 21.36(A) shows a confocal image of silica cells in maize (*Zea mays* L.). Silica cells also exhibit strong birefringence [Fig. 21.36(B)] (Sun *et al.*, 2001; Cheng *et al.*, 2003a; Chu *et al.*, 2003a) (Fig. 21.37).

Diatom frustules are also made of silica and can exhibit strong birefringent, scattering, and SHG properties (Fig. 21.38). In addition, calcium oxalate (Jauregui-Zuniga *et al.*, 2003), and calcium carbonate (in the form of calcite and argonite) and other mineral deposits (Homer and Wagner, 1992) are present in plant tissues and generally can be imaged by either BSL or by negative staining (filling the surrounding medium with fluorescent dye to "highlight" the non-fluorescing crystals) (Cheng and Kriete, 1995).

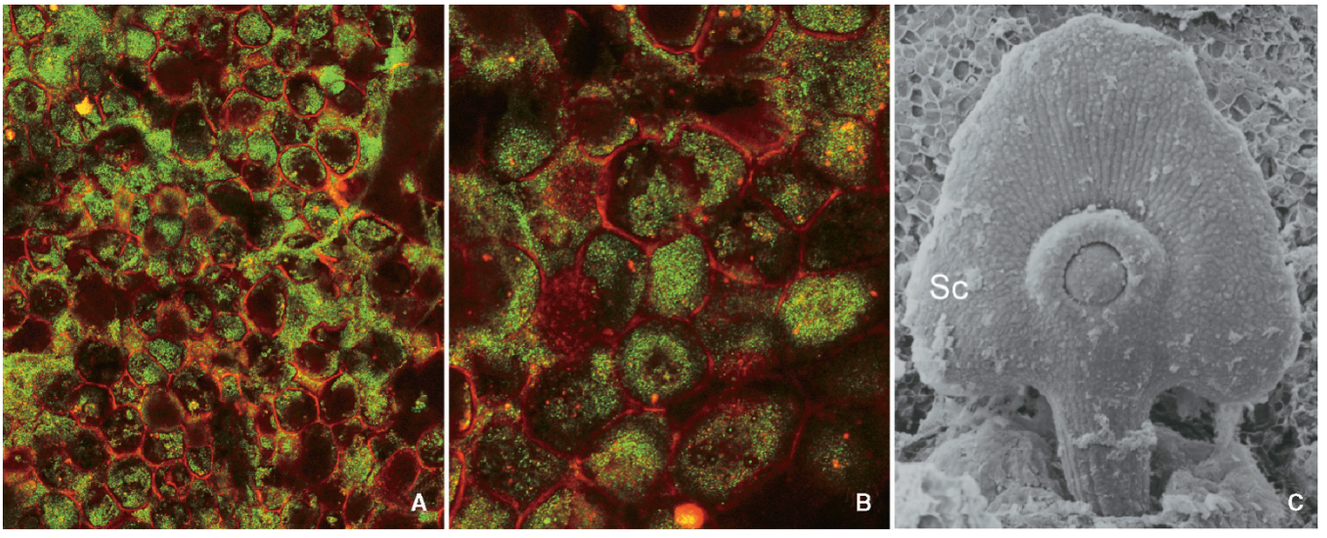

FIGURE 21.35. Two-channel confocal fluorescence image of maize scutellum showing the lipid and protein storage granules: (A) near surface, (B) 5 µm farther into the surface, (C) scanning electron microscope image of the same type of structure. Note the signal degrades rapidly in the tissue because of the high density of fluorescent features in the specimen.

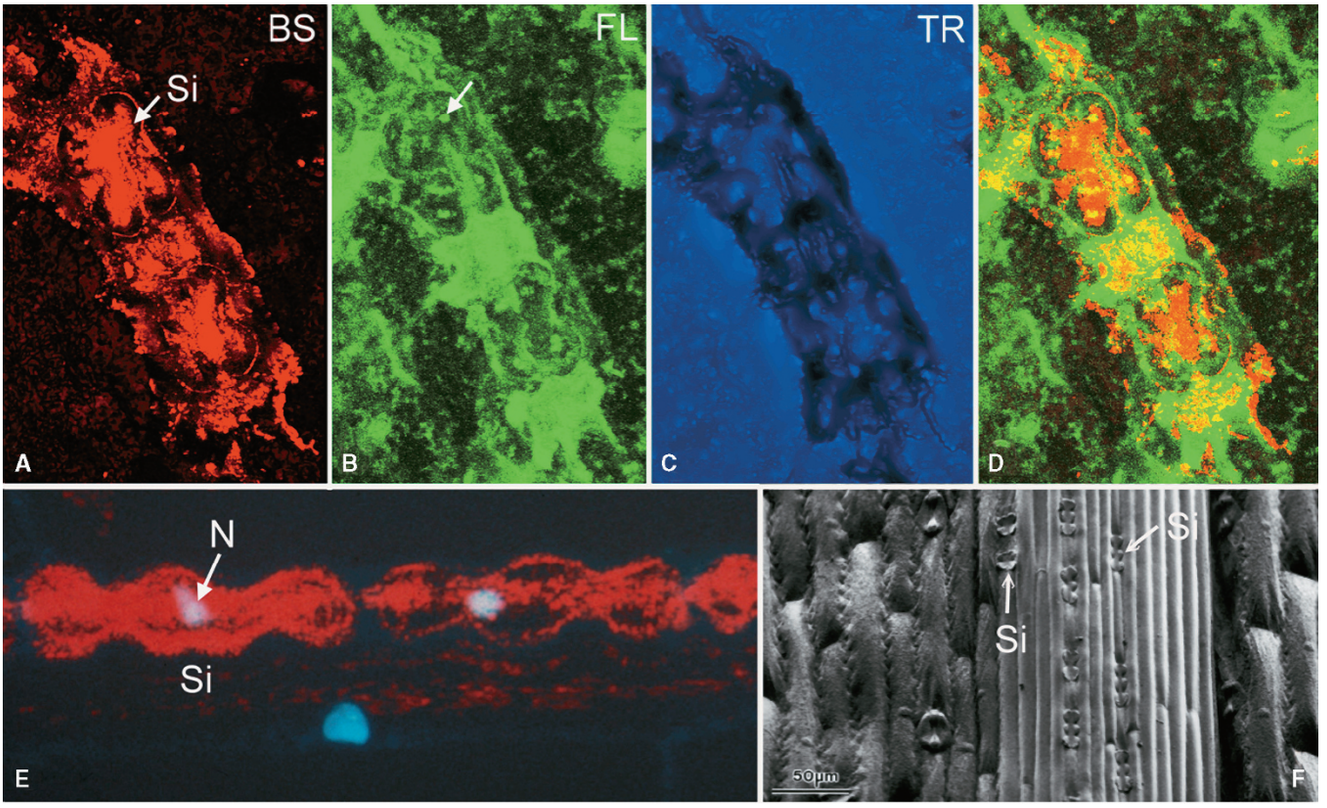

FIGURE 21.36. Silica cells in maize leaf. (A–D) $ZnCl_2$–HCl isolated cuticle with attached silica deposition imaged in (A) confocal backscattered light mode, (B) confocal autofluorescence mode (FL), and (C) conventional transmission image (TR). (D) False color combination of (A) and (B). The *arrow* in (B) indicates the center of the silica deposit and becomes visible in the isolated specimen. The isolated cuticle was mounted in water on a microscope slide. The significant difference in RI between silica and water provides the contrast in the conventional transmission image. (E) Silica cell stained in Feulgen showing the cell nuclei (N) in fluorescence mode (blue) and silica deposits in backscattered light mode (red). (F) SEM surface view (low-loss electron mode, LLE) of leaf surface showing the location of the silica cells (Si) (Wells and Cheng, 1992).

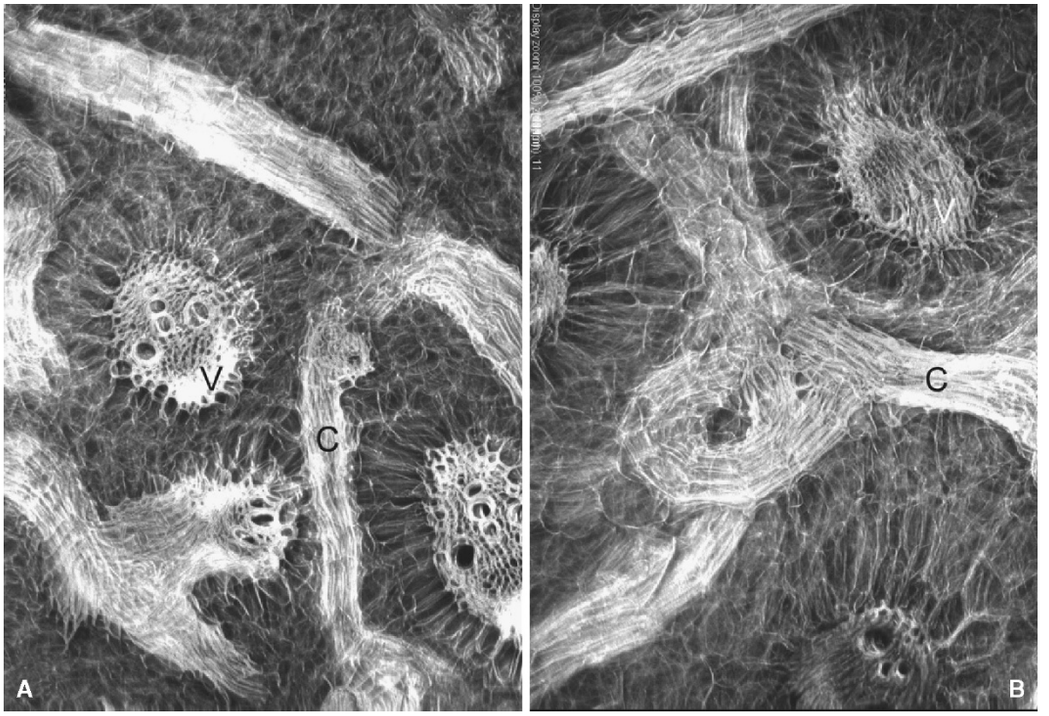

FIGURE 21.37. Two-photon, extended focus, fluorescence image of abnormal vasculature in a dwarf mutant, *na1/na1*, of maize (*Zea mays* L.) stained with analine blue. The secondary wall of the vascular bundles produce intense autofluorecence when excited with 780 nm NIR. V, vertically oriented vascular bundle; C, connecting bundle.

Primary and Secondary Cell Walls

Most plant cells are covered with an extracellular wall composed mainly of cellulose with additional lignins and sometimes, mineral deposits. Cellufluor (Polysciences) and other similar brighteners can be used in the study of cell walls in both UV confocal and multi-photon fluorescence microscopy. These dyes are frequently used for assaying cell wall regeneration of plant protoplasts and studying the development of tracheary elements (Taylor and Peterson, 2001). Cellufluor binds non-specifically to beta-linked polysaccharides such as chitin and cellulose. In addition, cellulose, carboxylated polysaccharides, beta-l, 3-glucans, pectin, callose, and certain other polysaccharides in the extracellular mucilages of root caps can be stained with Calcofluor White M2R [disodium salt of 4,4-bis-(4-anilino-bis-diethylamino-S-triazinyl-2-aminol)-2,2-stilbene-disulfonic acid; Hughes and McCully, 1975]. This fluorochrome stains most types of cell walls but usually not cell contents. Therefore, it is a useful dye for demarcating cellular boundaries and may also bind to lignin and some regions of starch grains. It has been reported that Calcofluor White M2R exhibits fluorescence dichroism: Two distinct colors are seen, depending on the relationship between the orientation of the structural elements in the wall and the polarization direction of the illumination (Hughes and McCully, 1975). If the plane of polarization of the illumination beam is known, one can study the orientation of the cell wall. Because at low concentration Calcofluor has no detectable effect on the root growth, it may also be used as a vital dye. A typical staining protocol follows.

Calcofluor Staining Procedure for Fixed and Fresh Tissue (Clark, 1981)

1. Fresh or 3% glutaraldehyde-fixed tissue can be used.
2. Stain the tissue in 0.01% Calcofluor solution for 20 to 60 s.
3. Destain in water for 1 min.
4. Mount in water for microscopy.

In contrast to the primary cell wall, the secondary wall contains less pectin and hemicellulose, but lignin and other components are still present. Lignin consists of polymerized phenylpropane units and acts as a structural component. The other non-structural components found in the secondary wall are tannins, oligosaccharides, and glycoproteins. Figure 21.37 shows a projection of the vasculature of a dwarf mutant of maize (*Zea mays* L., na1/na1 homozygous, Cheng *et al*., 2001b). Two-photon fluorescence imaging was used to achieve deep-tissue imaging at low magnification. In certain cells, such as the pollen mother cell at the Central Callose stage (Cheng *et al.*, 1979a), callosic wall is present. Callose is a helical molecule made of glucose units linked via 1,3 glycosidic linkages (callose contains also 1,4 and 1,6 linkages). Aniline blue binds to the helix, and the resulting complex produces yellow fluorescence.

Cell walls can exhibit strong birefringence and have been reported to have strong SHG properties (Cheng *et al.*, 2002b; Chu *et al.*, 2003a,b). The cell wall and the surrounding water are sufficiently different in RI to be capable of generating THG signals.

The structural components of the cell walls of algae consist of mannanes, xylanes, alginic acid, sulfonated polysaccharides, silicon, sporopollenin, and calcium carbonate (in the form of calcite and argonite). For those species with a high degree of mineralization, BSL mode is ideal for imaging the surface of the algae while fluorescence mode is used for cellular organelles. Figure 21.38 shows a diatom imaged in backscattered (silica surface) and fluorescence mode (chloroplast). Note that the particle (arrow) casts a shadow on the diatom below.

Fungi

Although fungi are not plants, and are usually classified as a separate kingdom, it is necessary to discuss the imaging of these important organisms here as many fungi are plant pathogens. Yeast and many other fungi have a highly reflective chitin surface and

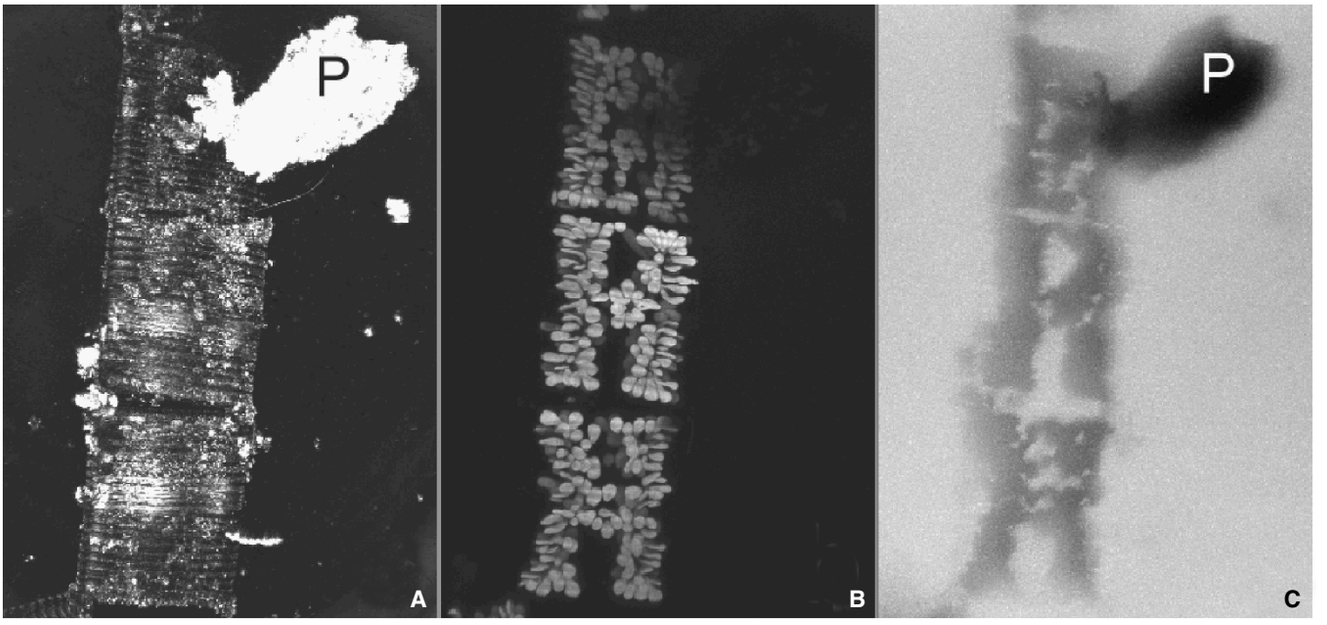

FIGURE 21.38. Fluorescence and backscattered light images of diatoms. (A) The silica wall produces an excellent backscattered light signal and (B) the chloroplasts emit strong autofluorescence. (C) Transmission image showing a soil particle (P) which casts a shadow in the fluorescence image (B) and produces strong scattering signal in the BSL image (A).

are frequently difficult to image. Imaging the penetration of fungal hyphae into plant tissue can also be challenging as hyphae often have a RI higher than the surrounding medium.

Chitin is a polymer that consists of glucose derivatives, *N*-acetyl glucosamine units connected by 1,4 linkages. Although occasionally found in algae, chitin is the main structural component in the cell wall of most fungi. Because Cellufluor binds non-specifically to beta-linked polysaccharides such as chitin and cellulose, high purity Cellufluor in deionized water (0.05% solution), with potassium hydroxide added as a clearing agent, can be used for the identification of various fungi. This dye is commercially available as Fungi-Fluor kit from Polysciences (Warrington, PA). Müller and Sengbusch (1983) have shown that Calcufluor white reveals the rhizoid system of the fungus *Blastocladiella anabaenae* on *Anabaena flosaquae* (a filamentous cyanobacteria).

CONCLUSION

Because plant cells contain light-scattering cell walls and a high concentration of pigments, they pose a challenge to both single-photon confocal and multi-photon fluorescence microscopy. In plant tissues free of pigmentation, two-photon fluorescence microscopy outperforms conventional single-photon confocal microscopy because of its increased depth penetration (Bhawalkar *et al.*, 1996; Cheng *et al.*, 1998). However, when the two-photon light is strongly absorbed, it can cause even more damage than single-photon excitation.

On the other hand, even heavily pigmented plant specimens do show significantly lower attenuation at wavelengths longer than 1000 nm, and therefore, long-wavelength two- and three-photon excitation can be considered. Results indicate that significant differences exist in fluorescence emission spectra between single-photon and two-photon excitation. Therefore, one should generally NOT select two-photon excitation wavelengths by simply doubling the wavelength of the linear absorption maximum of the fluorophore.

Mesophyll protoplast viability tests indicate that heavily pigmented (or heavily dye-loaded) plant cells can experience extensive photodamage under high-intensity NIR illumination. Even though photodamage is limited to the immediate vicinity of the focal point in two-photon fluorescence microscopy, overall cell viability is often lower than with single-photon confocal microscopy, assuming that the criterion is to obtain the same fluorescence signal level. Therefore, the choice of using single-photon confocal microscopy versus multi-photon fluorescence microscopy for plant material comes down to a careful analysis of attenuation and excitation spectra to determine which imaging modality is most likely to allow one to obtain the required information.

ACKNOWLEDGMENTS

Images presented in this chapter were obtained mostly from the author's laboratory at the State University of New York and at the National University of Singapore (NUS), where he is an adjunct professor of the Department of Biological Sciences (DBS). Most of the absorption and fluorescence spectra were prepared exclusively for this chapter using equipment at DBS-NUS. The author is grateful for the wonderful support and friendship from Professor Hew Choy Leong, Head of DBS-NUS and Professor Hanry Yu (Department of Physiology, NUS) during his 2003–2004 stay. The SHG work is a collaborative work with Professor Chi-kuang Sun of the Department of Electrical Engineering, National Taiwan University, Taipei, Republic of China. Some of the images used in this chapter were obtained by the author in demonstration experiments at the International 3D Microscopy of Living Cells Course (organized by Professor J. Pawley) held annually at the University of British Columbia, Canada. Special thanks to Dr. T. Holmes at AutoQuant for providing the Auto-Deblur deconvolution software and to Cambridge Research Instruments (Woburn, MA) for Figures 21.12 and 21.20. Thanks are also due to Nick White, Sir William Dunn School of Pathology, University of Oxford for his help editing the proofs.

REFERENCES

Agard, D.A., and Sedat, J.W., 1983, Three-dimensional architecture of a polytene nucleus, *Nature* 302:676–681.

Agard, D.A., Hiraoka, Y., Shaw, P., and Sedat, J.W., 1989, Fluorescence microscopy in three dimensions, *Meth. Cell Viol.* 30:353–377.

Bhawalkar, J.D., Shih, A., Pan, S.J., Liou, W.S., Swiatkiewicz, J., Reinhard, B.A., and Cheng, P.C., 1996, Two-photon laser scanning fluorescent microscopy – from a fluorophore and specimen perspective, *Bioimaging* 4:168–178.

Baker, E.A., 1982, Chemistry and morphology of plant epicuticular waxes, In: *The Plant Cuticle* (D.P. Cutler, K.L. Alvin, and C.E. Price, eds.), Academic Press, London, pp. 139–165.

Bianchi, G.P., and Salamini, F., 1975, Glossy mutants of maize, IV. Chemical composition of normal epicuticular waxes, *Maydica* 20:1–3.

Bianchi, G.P., Avato, P., and Salamini, F., 1977, Glossy mutant of maize. VII. Chemistry of glossy 7 epicuticular waxes, *Maydica* 22:9–17.

Bianchi, G.P., Avato, P., and Salamini, F., 1978, Glossy mutant of maize. IX. Chemistry of *glossy 4*, *glossy 8*, *glossy 15* and *glossy 18* surface waxes, *Heredity* 42:391–395.

Blaker, T.W., Greyson, R.I., and Walden, D.B., 1989, Variation among inbred lines of maize for leaf surface wax composition, *Crop Sci.* 29:28–32.

Bommineni, V.R., and Cheng, P.C., 1990, The use of confocal microscopy to study the developmental morphology of shoot apical meristems: A procedure to prepare the specimen. *Maize Genetic Cooperation Newsletter* 64:34.

Bommineni, V.R., Cheng, P.C., and Walden, D.B., 1995, Re-organization of cells in the maize apical dome within six days of culture after microsurgery, *Maydica* 40:289–298.

Bommineni, V.R., Cheng, P.C., Samarabandu, J.K., Lin, T.H., and Walden, D.B., 1993, Estimation of cell number in the maize apical meristematic dome and a three dimensional view of the reconstructed apical meristem by confocal microscopy and multidimensional image analysis, *Scanning* 15(Suppl. Ill):21–22.

Brininstool, G., 2003, A role for constitutive pathogen resistance in promoting cell expansion in *Arabidopis thaliana*, PhD thesis, Louisiana State University and Agricultural and Mechanical College, Baton Rouge, LA.

Brundrett, M.C., Murase, G., and Kendrick, B., 1990, Comparative anatomy of roots and mycorrhizae of common Ontario trees, *Can. J. Botany* 68: 551–578.

Carvalho, C.R., Saraiva, L.S., and Otoni, W.C., 2002, Maize root tip cell cycle synchronization, *Maize Genetic Cooperation Newsletter* 76:69.

Chen, I.-H., Chu, S.-W., Sun, C.-K., Lin, B.-L., and Cheng, P.C., 2002, Wavelength dependent damage in biological multi-photon confocal microscopy: A micro-spectroscopic comparison between femtosecond Ti:sapphire and Cr:forsterite laser sources, *Opt. Quantum. Electron*. 34:1251–1266.

Cheng, P.C., and Cheng, W.Y., 2001a, Artifacts in confocal and multi-photon microscopy, *Microsc. Microanal*. 7(Suppl. 2):1018–1019.

Cheng, P.C., and Kriete, A., 1995, Image contrast in confocal light microscopy, In: *Handbook of Biological Confocal Microscopy* (J.B. Pawley, ed.), Plenum Press, New York, pp. 267–281.

Cheng, P.C., and Walden, B., 2005, The cuticle of maize anther, *Microsc. Microanal.* Suppl. 2.

Cheng, P.C., Cheng, Y.K., and Huang, C.S., 1981, The structure of anther cuticle in rice *Oryza sativa* L., var. Taichung 65, *Natl. Sci. Council Monthly* 9:983–994.

Cheng, P.C., Greyson, R.I., and Walden, D.B., 1979a, Comparison of anther development in genic male-sterile (ms10) and in male-fertile corn (Zea mays) from light microscopy and scanning electron microscopy, *Can. J. Botany* 57:578–596.

Cheng, P.C., Greyson, R.I., and Walden, D.B., 1986, Anther cuticle of *Zea mays, Can. J. Botany* 64:2088–2079.

Cheng, P.C., Hibbs, A.R., Yu, H., Lin, P.C., and Cheng, W.Y., 2002, An estimate of the contribution of spherical aberration and self-shadowing in confocal and multi-photon fluorescent microscopy, *Microsc. Microanal*. 8(Suppl. 2):1068–1069.

Cheng, P.C., Lin, B.L., Kao, F.J., and Sun, C.K., 2000a, Multi-photon microscopy – Behavior of biological specimen under high intensity illumination, *SPIE Proc.* 4082:134–138.

Cheng, P.C., Lin, B.L., Kao, F.J., Sun, C.-K., and Johnson, I., 2000b, Multiphoton fluorescence spectroscopy of common nucleic acid probes, *Microsc. Microanal.* 6:820–821.

Cheng, P.C., Lin, B.L., Kao, F.J., Gu, M., Xu, M.-G., Gan, X., Huang, M.-K., and Wang, Y.-S., 2001, Multi-photon fluorescence microscopy – The response of plant cells to high intensity illumination, *Micron* 32:661–669.

Cheng, P.C., Newberry, S.P., Kim, H.G., Wittman, M.D., and Hwang, I.-S., 1990, X-ray contact microradiography and shadow projection microscopy, In: *Modern Microscopy* (P. Duke and A. Michette, eds.), Plenum Press, New York, pp. 87–117.

Cheng, P.C., Pareddy, D., Lin, T.H., Samarabandu, J.K., Acharya, R., Wang, and Liou, W.S., 1993, Confocal microscopy of botanical specimens, In: *Multi-Dimensional microscopy* (P.C. Cheng, T.H. Lin, W.L. Wu, and J.L. Wu, eds.), Springer-Verlag, New York, pp. 339–380.

Cheng, P.C., Pan, S.I., Shih, A., Kim, K.S., Liou, W.S., and Park, M.S., 1998, High efficient upconverters for multi-photon fluorescence microscopy, *J. Microsc.* 189:199–212.

Cheng, P.C., Sun, C.K., Cheng, P.C., and Walden, D.B., 2003*,* Nonlinear biophotonic crystal effect of opaline silica deposits in maize, *J. Scanning Microsc.* 235:80–81.

Cheng, P.C., Sun, C.K., Lin, B.L., and Chu, S.W., 2002, Bio-photonic crystal: SHG imaging, *Maize Genetics Cooperation Newsletter* 76:8–9.

Cheng, P.C., Walden, D.B., and Greyson, R.I., 1979b, Improved plant microtechnique for TEM, SEM and LM specimen preparation, *Natl. Sci. Council Monthly* 7:1000–1007.

Cheng, W.Y., Cheng, P.C., Gu, M., Gan, X.-S., and Walden, D.B., 2001b, The stem vasculature of *na1/na1* and *na2/na2* in *Zea mays, Scanning* 23:136–137.

Cheng, W.Y., Cheng, V.C., Cheng, P.C., and Walden, D.B., 2004, The orbicule in the anther of maize (*Zea mays* L.), *Scanning* 26:150–151.

Cheng, W.Y., Lee, T.C., and Cheng, P.C., 1999a, A loose-cell holder for confocal and multi-photon fluorescence microscopy, *Scanning* 21:61.

Cheng, W.Y., Lee, T.C., Walden, D.B., and Cheng, P.C., 1999b, Three-dimensional visualization of meiotic chromosomes in maize trisomy 6, *Microsc. Microanal.* 5(Suppl. 2):1262–1263.

Chu, S.W., Chen, I.S., Liu, T.M., Lin, B.L., Cheng, P.C., and Sun, C.K., 2001, Multi-modality nonlinear spectral microscopy based on a femtosecond Cr:Forsterite laser, *Opt. Lett.* 26:1909–1911.

Chu, S.W., Chen, I.S., Liu, T.-M., Sun, C.-K., Lin, B.L., Lee, S.P., Cheng, P.C., Liu, H.-L., Kuo, M-X., and Lin, D.-J., 2003, Nonlinear bio-photonic crystal effects revealed with multi-modal nonlinear microscopy, *J. Microsc.* 208:190–200.

Chu, S.W., Liu, T.M., Sun, C.K., Lin, C.Y., and Tsai, H.J., 2003, Real-time second-harmonic-generation microscopy based on a 2-GHz repetition rate Ti:sapphire laser, *Opt. Express* 11:933–938.

Clark, G., ed., 1981, *Staining Procedures*, Williams & Wilkins, Baltimore.

Crane, C.P., and Carman, J.G., 1987, Mechanisms of apomixis in *Elymus rectisetus* from eastern Australia and New Zealand, *Am. J. Botany* 72:477–496.

Cutler, D.P., Alvin, K.L., and Price, C.E., 1982, *The Plant Cuticle,* Academic Press, New York.

Dayanandan, P., Kaufman, P.B., and Franklin, C.I., 1983, Detection of silica in plants, *Am. J. Botany* 70:1079–1084.

Dawe, R.K., Agard, D.A., Sedat, J.W., and Cande, W.Z., 1992, Pachytene DAPI map, *Maize Genetics Cooperative Newsletter* 66:23–25.

Dickinson, H.G., and Bell, P.R., 1972, The role of the tapetum in the formation of sporopollenin-containing structures during microsporogenesis in *Pinus banksiana, Planta* (*Berl*.) 107:205–215.

Echlin, P., and Godwin, G., 1968, The ultras tructure and ontogeny of pollen in *Heleborus foetidus* L., I. The development of the tapetum and Ubisch body, *J. Cell Biol.* 3:161–174.

Federikson, M., 1992, The development of the female gametophyte of *Epipactis* (Orchidaceae) and its inference for reproductive ecology, *Am. J. Botany* 79:63–68.

Fricker, M.D., and White, N.S., 1992, Wavelength considerations in confocal microscopy of botanical specimens, *J. Microsc.* 166:29–42.

Greenspan, P., Mayer, E.P., and Fowler, S.D., 1985, Nile red: A selective fluorescent stain for intracellularlipid droplets, *J. Cell Biol.* 100:965–973.

Gu, M., Schilder, S., and Gan, X., 2000, Two-photon fluorescence image of microspheres embedded in turbid media, *J. Mod. Opt.* 47:959–965.

Herr, J.M. Jr., 1971, A new clearing squash technique for the study of ovule development in anger-sperms, *Am. J. Botany* 58:785–790.

Herr, J.M. Jr., 1974, A clearing-squash technique for the study of ovule and megagametophyte development in angiosperms, In: *Vascular Plant Systematics* (A.E. Radford, W.C. Dickison, J.R., Massey, and C.R. Bell, eds.), Harper & Row, New York.

Herr, J.M. Jr., 1985, The removal of phlobaphenes for improved clearing of sections and whole structures, *Am. J. Botany* 72:817.

Herr, J.M. Jr., 1992, Recent advances in clearing techniques for study of ovule and female gametophyte development, In: *Angersperm Pollen and Ovules* (E. Ottaviano, W.L. Mulcahy, M. SariGorIa, and G.B. Mulcahy, eds.), Springer-Verlag, New York, pp. 149–154.

Heslop-Harrison, J., and Dickinson, H.G., 1969, Time relationship of sporopollenin synthesis associated with tapetum and microspores in *Lilium, Planta* (*Berl*.) 84:199–214.

Hodson, M.J., and Sangster, A.G., 1988, Silica deposition in the inflorescence bracts of wheat *(Triticum aestivum)*, I. Scanning electron microscopy and light microscopy, *Can. J. Botany* 66:829–838.

Holloway, P.J., 1982, The chemical constitution of plant cutins, In: *The Plant Cuticle* (D. P. Cutler, K.L. Alvin, and C.E. Price, eds.), Academic Press, London, pp. 45–85.

Holloway, P.J., and Baker, E.A., 1968, Isolation of plant cuticles with zinc chloride-hydrochloric acid solution, *Plant Physiol.* 43:1878–1879.

Homer, H.T., and Wagner, B.L., 1992, Association of four different calcium crystals in the anther connective tissue and hypodermal stomium of *Capsicum annuum* (Sola-naceae) during microsporogenesis, *Am. J. Botany* 79:531–541.

Hose, E., Clarkson, D.T., Steudle, E., Schreiber, L., and Hartung, W., 2001, The exodermis: A variable apoplastic barrier, *J. Exp. Botany* 52:2245–2264.

Hughes, J., and McCully, M.E., 1975, The use of an optical brightener in the study of plant structure. *Stain Technol.* 50:319–329.

Huang, H.-C., and Chen, C.C., 1988, Genome multiplication in cultured protoplasts of two *Nicotiana* species, *J. Heredity* 79:28–32.

Johansen, D.A., 1940, *Plant Microtechnique*, McGraw-Hill, New York.

Jauregui-Zuniga, D., Eyes-Grajeda, J.P., Sepulveda-Sanchez, J.D., Whitaker, J.R., and Moreno, A., 2003, Crystallochemical characterization of calcium oxalate crystals, *J. Plant Physiol*. 160:239–245.

Jones, L.H.P., and Handreck, K.A., 1967, Silica in soils, plants and animals, *Adv. Agron.* 19:107–149.

Juniper, B.E., and Jeffree, C.E., 1983, *Plant Surfaces*, Edward Arnold, London.

Kao, F.J., Lin, B.L., and Cheng, P.C., 2000a, Multi-photon fluorescence microspectroscopy *SPIE Proc.* 3919:2–8.

Kao, F.J., Wang, Y.S., Huang, W.W., Huang, S.L., and Cheng, P.C., 2000b, Second-harmonic generation microscopy of tooth, *SPIE Proc.* 4082:119–124.

Kao, F.J., Cheng, P.C., Sun, C.-K., Lin, B.L., Wang, Y.-M., Chen, J.-C., Wang, Y.-S., Liu, T.-M., and Huang, M.-K., 2000c, Multi-photon spectroscopy of plant tissues, *Scanning* 22:193–195.

Kennedy, S.M., and Lytle, F.E., 1986, P-Bis(o-methylstytyl)benzene as a power squared tensor for two-photon absorption measurement between 537 and 694 nm, *Anal. Chem*. 58:2643–2647.

Kim, H.G., Cheng, P.C., Wittman, M.D., and Kong, H.J., 1990, Pulsed X-ray contact microscopy and its applications to structural and developmental botany, In: *X-Ray Microscopy in Biology and Medicine* (K. Shinohara, ed.), Springer-Verlag, New York, pp. 233–242.

Kirk, P.Kl. Jr., 1970, Neutral red as a lipid fluorochrome, *Stain Technol.* 45: 1–4.

Konig, K.H., Liang, H., Berns, M.W., and Tromberg, B.J., 1995, Cell damage by near-IR microbeams, *Nature* 377:20–21.

Konig, K., Liang, H., Berns, M.W., and Tromberg, B.J., 1996a, Cell damage in near-infrared multimode optical traps as a result of multi-photon absorption, *Opt. Lett*. 21:1090–1092.

Konig, K., So, P.T.C., Mantulin, W.W., and Gratton, E., 1997, Cellular response to near-infrared femtosecond laser in two-photon microscopes, *Opt. Lett.* 22:135–136.

Konig, K., So, P.T.C., Mantulin, W.W., Tromberg, B.J., and Gratton, E., 1996b, Two-photon excitation lifetime imaging of autofluorescence in cell during UVA and NIR photostress, *J. Microsc.* 183:197–204.

Lide, D.R., ed., 1991, *Handbook of Chemistry and Physics*, CRC Press, Boca Raton, Florida, pp. 7–29.

Lin, B.L., Cheng, P.C., and Sun, C.-K., 2001, Optical density of leaf, *Maize Genetics Cooperation Newsletter* 75:61–62.

Lin, B.L., Kao, F.J., Cheng, P.C., and Cheng, W., 2000a, The response of maize protoplasts to high intensity illumination in multi-photon fluorescence microscopy, *Microsc. Microanal.* 6(Suppl. 2):806–807.

Lin, B.L., Kao, F.J., Cheng, P.C., Chen, R.W., Huang, M.K., Wang, Y.S., Chen, J.C., Wang, Y.S., and Cheng, W.Y., 2000b, The response of maize protoplast in multi-photon fluorescent microscopy, *Scanning* 22:196–197.

Lin, B.L., Kao, F.J., Sun, K.-C., and Cheng, P.C., 2000c, Absorption and multi-photon excited fluorescence properties of maize tissue, *Maize Genetics Cooperation Newsletter* 74:63–64.

Müller, U., and Sengbusch, P.v., 1983, Interactions of species in an *Anabaena flosaque* association from the Plußsee (East-Holstein, Federal Republic of Germany). Studies by use of fluorescent markers, *Oecologia* 58: 215.

Oehring, H., Riemann, I., Fischer, P., Halbhuber, K.-J., and König, K., 2000, Ultrastructure and reproduction behaviour of single CHO-K1 cells exposed to near infrared femtosecond laser pulses, *Scanning* 22:263.

Pace, G.M., Reed, J.N., Ho, L.C., and Fahey, J.W., 1987, Anther culture of maize and the visualization of embryogenic microspores by fluorescent microscopy, *Theor. Appl. Genet*. 73:863–869.

Palser, B.F., Rouse, J.L., and Williams, E.G., 1989, Coordinated timetables for mega-gametophyte development and pollen tube growth in *Rhododendron nuttalli* from anthesis to early post-fertilization, *Am. J. Botany* 76:1167–1202.

Pareddy, D.R., Greyson, R.I., and Walden, D.B., 1989, Production of normal, germinable and viable pollen from *in vitro* cultured maize tassels, *Theor. Appl. Genet.* 77:521–526.

Pawley, J.B., 2002, Limitations on optical sectioning in live-cell confocal microscopy, *Scanning* 24:241.

Schilders, S.P., and Gu, M., 2000, Limiting factors on image quality in imaging through turbid media under single-photon and two-photon excitation, *Microsc. Microanal*. 6:156–160.

Stelly, D.M., Peloquin, S.J., Palmer, R.G., and Crane, C.F., 1984, Mayor's hemalum-methyl salicylate: a stain-clearing technique for observations within whole ovules. *Stain Technol.* 59:155–161.

Sun, C.K, Chu, S.W., Liu, T.M., and Cheng, P.C., 2001, High intensity scanning microscopy with a femtosecond Cr:Forsterite laser, *Scanning* 22:95–96.

Taylor, J.H., and Peterson, C.A., 2001, Maturation of the tracheary elements in the roots of *Pinus banksiana* and *Eucalyptus grandis*, *Can. J. Botany* 79:844–849.

Tulloch, A.P., 1981, Composition of epicuticular waxes from 28 genera of Gramineas: Differences between subfamilies, *Can. J. Botany* 59:1213–1221.

Vergne, P., Delvallee, I., and Dumas, C., 1987, Rapid assessment of microspore and pollen development stages in wheat and maize using DAPI and membrane permeabilization, *Stain Technol.* 62:299–304.

Young, B.A., Sherwood, R.T., and Bashaw, E.C., 1979, Cleared-pistil and thick-sectioning techniques for detecting aposporous apomixis in grasses, *Can. J. Botany* 57:1668–1672.

Wells, O.C., and Cheng, P.C., 1992, High-resolution backscattered electron images in the scanning electron microscope, *Proc. EMSA* 50:1608–1609.

White, N.S., Errington, R.J., Wood, J.L. and Fricker, M.D., 1996, Quantitative measurements in multidimensional, botanical fluorescence images, *J. Microsc.* 181(2):99–116.